

1        **Enhanced light absorption and reduced snow albedo due to**  
2                    **internally mixed mineral dust in grains of snow**

3        Tenglong Shi<sup>1</sup>, Jiecan Cui<sup>1</sup>, Yang Chen<sup>1</sup>, Yue Zhou<sup>1</sup>, Wei Pu<sup>1</sup>, Xuanye Xu<sup>2</sup>, Quanliang  
4                    Chen<sup>2</sup>, Xuelei Zhang<sup>3</sup>, and Xin Wang<sup>1,4</sup>

5        <sup>1</sup>Key Laboratory for Semi-Arid Climate Change of the Ministry of Education, College  
6        of Atmospheric Sciences, Lanzhou University, Lanzhou 730000, China

7        <sup>2</sup>College of Atmospheric Sciences, Chengdu University of Information Technology,  
8        Chengdu 610225, China

9        <sup>3</sup>Key laboratory of Wetland Ecology and Environment, Northeast Institute of  
10        Geography and Agroecology, Chinese Academy of Sciences, Changchun 130102,  
11        China

12        <sup>4</sup>Institute of Surface-Earth System Science, Tianjin University, Tianjin 300072, China

13

14        Corresponding author: Xin Wang (wxin@lzu.edu.cn)

15

1 **Abstract.** Mineral dust is a major light-absorbing aerosol, which can significantly  
2 reduce snow albedo and accelerate snow/glacier melting via wet and dry deposition on  
3 snow. In this study, three scenarios of internal mixing of dust in ice grains were  
4 analyzed theoretically by combining asymptotic radiative transfer theory and  
5 (core/shell) Mie theory to evaluate the effects on absorption coefficient and albedo of  
6 the semi-infinite snowpack consisting of spherical snow grains. In general, snow albedo  
7 was substantially reduced at wavelengths of  $<1.0 \mu\text{m}$  by internal dust–snow mixing,  
8 with stronger reductions at higher dust concentrations and larger snow grain sizes.  
9 Moreover, calculations showed that a non-uniform distribution of dust in snow grains  
10 can lead to significant differences in the values of the absorption coefficient and albedo  
11 of dust-contaminated snowpack at visible wavelengths relative to a uniform dust  
12 distribution in snow grains. Finally, using comprehensive in situ measurements across  
13 the Northern Hemisphere, we found that broadband snow albedo was further reduced  
14 by 5.2% and 9.1% due to the effects of internal dust–snow mixing on the Tibetan  
15 Plateau and North American mountains. This was higher than the reduction in snow  
16 albedo caused by black carbon in snow over most North American and Arctic regions.  
17 Our results suggest that significant dust–snow internal mixing is important for the  
18 melting and retreat of Tibetan glaciers and North American mountain snowpack.  
19

## 1 **1. Introduction**

2 Snow cover is one of the most reflective surfaces in the Earth system, and plays a crucial  
3 role in the atmospheric solar radiation energy budget via snow albedo feedbacks (Di  
4 Mauro et al., 2020; Flanner et al., 2011; Jacobson, 2004; Usha et al., 2020; Xie et al.,  
5 2018). Previous studies have shown that light-absorbing particles (LAPs) effectively  
6 reduce snow albedo and enhance the absorption of solar radiation after deposition, these  
7 studies were based on in situ observations and model simulations (Casey et al., 2017;  
8 Hadley and Kirchstetter, 2012; Shi et al., 2020; Warren and Wiscombe, 1980; Yasunari  
9 et al., 2012; Yasunari et al., 2015). As a result, snow contaminated with LAPs shows  
10 significant changes in morphology (Niwano et al., 2012; Rango et al., 1996), chemistry  
11 (France et al., 2012; Reay et al., 2012), hydrology (Matt et al., 2018; Qian et al., 2015;  
12 Rahimi et al., 2019), snowmelt rate (Kaspari et al., 2015; Warren, 1984;), and radiative  
13 properties (Grenfell et al., 2002; Hansen and Nazarenko, 2004; Zhao et al., 2014).

14 Numerous studies have assessed the potential effects of LAPs, such as black carbon  
15 (BC) and mineral dust, on snow albedo by assuming that LAPs mixed outside spherical  
16 snow grains (i.e., external mixing) (Flanner et al., 2007; Kokhanovsky, 2013; Libois et  
17 al., 2013; Wang et al., 2017; Warren and Wiscombe, 1980). For example, Warren and  
18 Wiscombe (1980) calculated snow spectral albedo by solving a radiative transfer  
19 equation using Mie theory and  $\delta$ -Eddington approximations, and found that 10–100 ng  
20  $\text{g}^{-1}$  of BC and 1–10  $\mu\text{g g}^{-1}$  of dust in old snow decreased albedo by 1%–7% and 2%–  
21 10% at 400 nm wavelength, respectively. Flanner et al. (2007) pointed out that the  
22 reduction in snow albedo for 1000 ng  $\text{g}^{-1}$  BC in snow was 0.045 (0.17) with a 50 (1000)  
23  $\mu\text{m}$  snow grain radius ( $R_{\text{ef}}$ ) based on the Snow, Ice, and Aerosol Radiation (SNICAR)  
24 radiative transfer model. This model utilizes theory from Wiscombe and Warren (1980)  
25 and the two-stream radiative transfer solution from Toon et al. (1989). Wang et al. (2017)  
26 developed a Spectral Albedo Model for Dirty Snow (SAMDS) based on asymptotic  
27 radiative transfer theory, which is a function of the snow grain radius, LAP (e.g., BC,  
28 dust) mixing ratios, and the mass absorption coefficients (MACs) of LAPs. Their results

1 revealed that broadband snow albedo decreased 0.03 and 0.003 due to 200 ng g<sup>-1</sup> of BC  
2 and 2 μg g<sup>-1</sup> of dust in snow, respectively, with a R<sub>ef</sub> of 200 μm. Additionally, recent  
3 studies found that snow nonsphericity can interact with LAP-snow mixing, which leads  
4 to weaker LAP-induced albedo reductions for nonspherical snow shapes than snow  
5 spheres (e.g., Dang et al., 2016; He et al., 2018, 2019).

6 Recently, direct snowpack observations have shown evidence for the existence of LAP–  
7 snow internal mixing (e.g., Horhold et al., 2012; Spaulding et al., 2011). LAPs tend to  
8 mix externally with snow grains through dry deposition and/or below cloud scavenging,  
9 while internal LAP–snow mixing can be produced by nucleation, accretion, riming,  
10 aggregation, and sintering during aerosol–cloud–precipitation processes (i.e., wet  
11 deposition; Figure 1) (Flanner et al., 2012). Furthermore, Flanner et al. (2012) found  
12 that internal BC/ice mixing (IBM) increased the absorption of snowpack by a factor  
13 1.8–2.1 relative to external BC/ice mixing (EBM). He et al. (2018) indicated that IBM  
14 enhanced the mean snow albedo reduction over the Tibetan plateau by 30%–60%  
15 relative to EBM, based on the updated SNICAR model. Additionally, Dombrovsky and  
16 Kokhanovsky (2020) demonstrated that non-uniform BC distribution in ice grains may  
17 lead to significantly different absorption coefficients and snowpack albedo in visible  
18 (VIS) wavelengths.

19 Numerous studies have addressed the role of IBM in enhancing the absorption of  
20 snowpack due to its strong absorption effect relative to other LAPs (Dombrovsky and  
21 Kokhanovsky, 2020; Flanner et al., 2012; He et al., 2018; Liou et al., 2011). In contrast,  
22 few studies have considered the effects of internal dust/ice mixing (IDM) in snowpack.  
23 Liou et al. (2014) is the pioneer to investigate the dust-snow internal mixing effects  
24 based on the geometric-optics surface-wave approach. Subsequently, He et al. (2019)  
25 used the same method to explicitly quantify the combined effects of dust-snow internal  
26 mixing and snow grain nonsphericity on snow optical properties, thereafter, develop a  
27 set of new dust-snow parameterizations for land/climate modeling applications for the  
28 first time. Actually, dust particles are generally larger than BC, and act as more efficient

1 ice nuclei, showing a better ability to influence cloud formation and precipitation  
2 (Creamean et al., 2013; Huang et al., 2014). Therefore, they are more likely to mix  
3 internally with ice grains. Furthermore, dust can also dominate light absorption and  
4 effectively decrease snow albedo because of its relatively high mass abundance (ppm)  
5 in snowpack, especially in areas with seasonal and patchy snow cover or mountainous  
6 regions (Di Mauro et al., 2015; Gabbi et al., 2015; Painter et al., 2012; Reynolds et al.,  
7 2020; Xie et al., 2018). Therefore, it is important to account for IDM when estimating  
8 the impact of dust deposition on snow albedo.

9 In this study, we assess the effects of external/internal mixing of dust with ice grains on  
10 the snowpack absorption coefficient and albedo using asymptotic radiative transfer  
11 theory and Mie theory. In addition, the uniformity and nonuniformity of dust particle  
12 distribution inside ice grains are considered for IDM based on the effective medium  
13 approximation, and the combined effects of dust content and snow grain radius on snow  
14 albedo are quantified. A schematic of various dust spatial distributions from this study  
15 is presented in Figure 2. We further discuss snow albedo sensitivity to complex  
16 refractive indices and dust particle size distribution. Based on a comprehensive set of  
17 field measurements of dust concentrations, we estimate the reductions in snow albedo  
18 by dust external/internal mixing with ice grains across the Northern Hemisphere.

## 19 **2 Methods**

### 20 **2.1 External mixing model**

21 For fairly pure snow, semi-infinite means about 20 cm in the VIS and 3 cm in the near-  
22 infrared (NIR) regions of snow depths, respectively (Zhou et al., 2003). For a semi-  
23 infinite snow layer under diffuse illumination conditions, albedo can be calculated  
24 using an asymptotic analysis of radiative transfer theory, which is valid in small  
25 absorptions (Kokhanovsky and Zege, 2004; Zege et al., 1991):

$$26 \alpha_{\lambda} = \exp(-4S_{\lambda}) \quad (1)$$

27 where  $\alpha_{\lambda}$  is the spectral snow albedo,  $\lambda$  is the wavelength,  $S_{\lambda}$  is the similarity

1 parameter, and

$$2 \quad S_\lambda = \sqrt{\frac{\sigma_{abs}}{3\sigma_{ext}(1-g)}} \quad (2)$$

3 In Eq. (2),  $\sigma_{abs}$  and  $\sigma_{ext}$  are the absorption and extinction coefficients, respectively,  
4 and  $g$  is the asymmetry parameter (the average cosine of the phase function of the  
5 medium).

6 According to Eq. (18) and (25) in Kokhanovsky and Zege (2004), the extinction  
7 coefficients of particles can be expressed as:

$$8 \quad \sigma_{ext} = \frac{1}{l_{tr}(1-g)} = \frac{3C_v}{2r_{ef}} \quad (3)$$

9 where  $l_{tr}$  is the photon transport path length,  $C_v = \rho_{snow}/\rho_{ice}$  is the volumetric  
10 snow particle concentration, and the values  $\rho_{ice} = 916.7 \text{ kg m}^{-3}$  and  $\rho_{snow} = 300 \text{ kg}$   
11  $\text{m}^{-3}$  are used in subsequent calculations.  $r_{ef}$  is the effective snow grain radius, which  
12 is equal to the radius of the volume-to-surface equivalent sphere ( $r_{ef} = \frac{3\bar{V}}{4\bar{A}}$ ) where  $\bar{V}$   
13 and  $\bar{A}$  are the average volume and cross-sectional (geometric shadow) area of snow  
14 grains, respectively.

15 For external dust/ice mixing (EDM) in a dust-contaminated snowpack, the total  
16 absorption coefficient ( $\sigma_{abs}$ ) can be derived from the absorptions by snow ( $\sigma_{abs}^{snow}$ ) and  
17 dust ( $\sigma_{abs}^{dust}$ ):

$$18 \quad \sigma_{abs} = \sigma_{abs}^{snow} + \sigma_{abs}^{dust} \quad (4)$$

19 For example, consider a hypothetical case of snow composed of monodispersed,  
20 spherical grains of ice. Although non-spherical snow grains lead to a slight increase in  
21 snow albedo, Dang et al. (2016) found that the albedo of a snowpack consisting of non-  
22 spherical snow grains can be mimicked by using smaller, spherical grains; thus, we do  
23 not consider the effect of non-spherical snow grains in this study. Therefore, we used  
24 the following equation for the absorption coefficient of snow (Dombrovsky and Baillis,  
25 2010):

$$26 \quad \sigma_{abs}^{snow} = \frac{0.75C_v \cdot Q_{abs}^{ice}}{r_{ef}} \quad (5)$$

27 where  $Q_{abs}^{ice}$  is the efficiency factor of absorption for a single ice grain, and the value

1 of  $Q_{abs}^{ice}$  can be calculated for homogeneous spherical ice grains considered in classical  
 2 Mie theory.

3 The absorption coefficient of dust (Aoki et al., 2000; Marley et al., 2001; Warren et al.,  
 4 2006) is expressed as:

$$5 \quad \sigma_{abs}^{dust} = \frac{Q_{abs}^{dust} \cdot \pi \cdot (r_{ef}^{dust})^2}{\frac{4}{3} \pi \cdot (r_{ef}^{dust})^3} \cdot C_{dust} = \frac{3Q_{abs}^{dust}}{4r_{ef}^{dust}} \cdot C_{dust} = MAC_{abs}^{dust} \cdot \rho_{dust} \cdot C_{dust} \quad (6)$$

6 where  $Q_{abs}^{dust}$  and  $MAC_{abs}^{dust}$  is the absorption efficiency and MAC of dust,  
 7 respectively, that can be obtained via Mie theory, and  $\rho_{dust}$  and  $r_{ef}^{dust}$  represent the  
 8 density and effective dust radius, respectively. In this study,  $\rho_{dust}$  was assumed to be  
 9  $2500 \text{ kg m}^{-3}$  (Zender et al., 2003). We also assumed a log-normal dust size distribution  
 10 with a geometric mean diameter of  $0.65 \text{ }\mu\text{m}$  and standard deviation of 2.0 (equivalent  
 11 to an effective radius of  $1.1 \text{ }\mu\text{m}$ ), which represents dust from large-scale transport  
 12 (Formenti et al., 2011; Maring et al., 2003) that is likely smaller in size than from local  
 13 soil (Kok, 2011). The effects of dust size on snow optical properties and albedo were  
 14 further quantified through sensitivity simulations (see section 3.4). Dust volumetric  
 15 concentrations ( $C_{dust}$ ) are expressed as:

$$16 \quad C_{dust} = \frac{\rho_{snow} \cdot C_{dust}^*}{\rho_{dust}} \quad (7)$$

17 where  $C_{dust}^*$  is the mass concentration of dust in snow ( $\text{kg kg}^{-1}$ ). Thus, the spectral  
 18 albedo of dust-contaminated snow for EDM can be easily calculated with Eq. (1) to (7).

## 19 **2.2 Internal mixing model**

20 For the IDM (Figure 2), we first determined the effective optical constants of ice  
 21 containing small dust particles via an effective medium approximation (Maxwell-  
 22 Garnett and Larmor, 1904). According to this approach, the complex permittivity of a  
 23 composite medium in ice grains can be calculated in terms of particle polarizability by  
 24 applying the Lorentz-Lorenz formula (Koledintseva et al., 2009; Markel, 2016). We  
 25 used the following relationships to calculate effective complex refractive indices (RIs),  
 26  $m_{ef} = n_{ef} - ik_{ef}$  at known values of  $m_{ice} = n_{ice} - ik_{ice}$  for pure ice and  $m_{dust} = n_{dust} - ik_{dust}$

1 for dust:

$$2 \quad m_{ef}^2 = m_{ice}^2 \frac{2\delta_{dust}(m_{dust}^2 - m_{ice}^2) + m_{dust}^2 + 2m_{ice}^2}{2m_{ice}^2 + m_{dust}^2 - \delta_{dust}(m_{dust}^2 - m_{ice}^2)} \quad (8)$$

3 where  $\delta_{dust}$  is the local dust fraction volume in an ice grain. We obtained the spectral  
 4 complex RIs of ice from Warren and Brandt (2008) and the spectral complex RIs of  
 5 dust from Dang et al. (2015). The imaginary part of the complex RIs of ice ( $k_{ice}$ ) and  
 6 dust ( $k_{dust}$ ) associated with absorption is shown in Figure 3. We also evaluated the effect  
 7 of dust on the imaginary part of the effective complex RIs ( $k_{ef}$ ) assuming dust mass  
 8 concentrations ( $C_{dust}^*$ ) of 1–100 ppm (or  $\mu\text{g g}^{-1}$ ) in snow.

9 In all variations of the spatial distribution of dust particles in snow, the dust mass  
 10 concentration was assumed to be constant, which means that the local dust fraction  
 11 volume may differ. In an example of spherical ice grains with uniformly distributed  
 12 dust, the dust fraction volume in an ice grain was determined as:

$$13 \quad \delta_{dust}^0 = \frac{C_{dust}^* \rho_{ice}}{C_v \rho_{dust}} \quad (9)$$

14 where the ratio of  $C_{dust}^*/C_v$  is the mass fraction of dust in the ice grain.

15 We considered two cases of non-uniform dust distributed in a spherical ice grain with  
 16 radius  $r_{ef}$ : (1) We assumed that the same mass of dust is uniformly distributed in the  
 17 central part of the ice grain ( $r_{ef}^{dust} < r_c \leq r_{ef}$ ). (2) We assumed all of the dust was in  
 18 the surface layer of the ice grain ( $r_{ef}^{dust} < r_p \leq r_{ef}$ ) (Figure 2). In both cases the local  
 19 value of  $\delta_{dust}$  increases as:

$$20 \quad \delta_{dust} = \delta_{dust}^0 / \psi \quad \psi = \begin{cases} \bar{r}_c^3 & \text{central pollution} \\ 1 - (1 - \bar{r}_p)^3 & \text{peripheral pollution} \end{cases} \quad (10)$$

21 where  $\bar{r}_c = r_c/r_{ef}$  and  $\bar{r}_p = r_p/r_{ef}$ .  $\bar{r}_c = 1$  and  $\bar{r}_p = 1$  correspond to uniformly  
 22 distributed dust when  $\psi = 1$  and  $\delta_{dust} = \delta_{dust}^0$ , and  $\psi < 1$  and  $\delta_{dust} > \delta_{dust}^0$  in  
 23 other cases. Obviously, dust particles increase the imaginary part of the effective  
 24 complex RIs in polluted ice grains (Figure 3).

25 In summary, the  $m_{ef}$  of a spherical ice grain with uniformly and non-uniformly  
 26 distributed , according to Eq. (8) to (10), then their corresponding absorption



1 efficiencies can be obtained using classical Mie theory and core/shell Mie theory,  
2 respectively. The spectral snow albedo for IDM can be easily calculated using Eq. (1)  
3 to (5).

### 4 **2.3 Broadband snow albedo calculations**

5 The spectral albedo ( $\alpha_\lambda$ ) is integrated over the solar spectrum ( $\lambda = 300\text{--}2500$  nm) and  
6 weighted by incoming solar irradiance ( $E_\lambda$ ) to calculate broadband snow albedo (Hadley  
7 and Kirchstetter, 2012):

$$8 \quad \alpha_{integrated} = \frac{\int \alpha_\lambda E_\lambda d\lambda}{\int E_\lambda d\lambda} \quad (11)$$

9 Following the study of Dang et al. (2017), the incoming solar irradiance we used is a  
10 typical surface solar spectrum at mid to high latitudes from January to March under the  
11 cloudy sky, calculated by the Santa Barbara DISORT Atmospheric Radiative Transfer  
12 (SBDART) model (Pu et al., 2019). The SBDART model is a widely used atmospheric  
13 radiation transfer model based on a collection of highly developed physical models,  
14 including the Discrete Ordinate Radiative Transfer module (Stamnes et al., 1988), low-  
15 resolution atmospheric transmission models, and Mie theory. The SBDART model can  
16 be used to compute radiative transfer at different heights and directions under both clear  
17 and cloudy sky conditions. Details on the SBDART model can be found in Ricchiazzi  
18 et al. (1998).

### 19 **2.4 Dust concentration measurements**

20 To estimate the effect of dust on snow albedo in real snowpack, we collected a  
21 comprehensive set of in situ dust concentration measurements during field campaigns  
22 to Inner Mongolia, China (IMC) (Wang et al., 2013), the Tibetan Plateau (TP) (Li et al.,  
23 2017, 2018; Li et al., 2016, 2019; Niu et al., 2017; Qu et al., 2014; Zhang et al., 2017,  
24 2018), Sapporo, Japan (SJ) (Kuchiki et al., 2015), the European Alps (EP) (Di Mauro  
25 et al., 2015; Lim et al., 2014), and North American mountains (NAM) (Painter et al.,  
26 2012; Reynolds et al., 2020). The field campaigns conducted in the TP can be further  
27 grouped into three regions, as in previous  $\delta^{18}\text{O}$  precipitation studies (Yao et al., 2013).

1 These three distinct domains were associated with the Indian monsoon (Southern TP),  
2 westerlies (Northern TP), and transition (Central TP) (Yao et al., 2013). It is worth  
3 noting that we only considered regions with higher dust concentrations ( $>1$  ppm), such  
4 that polar regions are not included in this study. Measurements of dust in the snow  
5 samples were generally obtained by weighing the filter before and after filtration using  
6 a microbalance.

### 7 **3. Results**

#### 8 **3.1 Impact on the imaginary part of the effective complex RIs**

9 We evaluated the effect of dust on  $k_{ef}$ , including  $k_{ice}$  and  $k_{dust}$  associated with absorption  
10 (Figure 3). The  $k_{dust}$  was in a narrow range ( $\sim 0.001$ – $0.01$ ) and gradually decreased with  
11 increasing wavelength in the ultraviolet (UV) and VIS regions, then remained stable in  
12 the NIR band. The  $k_{ice}$  varied by eight orders of magnitude from the UV ( $\sim 10^{-11}$ ) to NIR  
13 ( $\sim 10^{-3}$ ) bands, and increased with increasing wavelength, except at  $1.03 \mu\text{m}$  where  $k_{ice}$   
14 decreased slightly as a result of the presence of ice absorption features (Warren, 2019).  
15 Figure 3 also shows the  $k_{ef}$  with dust mass concentrations ranging from 1 to 100 ppm  
16 and wavelengths of 300–1500 nm. The  $k_{ef}$  clearly varied depending on the wavelength  
17 and increased with dust mass concentrations. For a given dust mass concentration,  $k_{ef}$   
18 decreased with wavelengths from UV to VIS, then increased from VIS to NIR. For  
19 example, the value of  $k_{ef}$  decreased from  $4.26 \times 10^{-8}$  at 300 nm to  $1.36 \times 10^{-8}$  at 500  
20 nm, then rose to  $1.73 \times 10^{-6}$  at 1000 nm at a dust concentration of 10 ppm. Moreover,  
21 the wavelength of the minimum of  $k_{ef}$  varied from  $\sim 500$  nm to  $\sim 650$  nm depending on  
22 the dust mass concentrations (1 to 100 ppm). Additionally, it is worth noting that  $k_{ef}$  was  
23 not sensitive to dust mass concentrations in wavelengths  $>1000$  nm, which was  
24 generally consistent with  $k_{ice}$ , because the difference between  $k_{dust}$  and  $k_{ice}$  is more than  
25 compensated by the much larger difference in ice and dust concentration at those  
26 wavelengths. Conversely,  $k_{ef}$  showed significant differences relative to  $k_{ice}$  in the UV  
27 and VIS regions, with higher dust mass concentrations demonstrating larger differences.

1 For example,  $k_{ef}$  was enhanced by 3, 21, and 205 times at 500 nm relative to  $k_{ice}$  for dust  
2 mass concentrations of 1, 10, and 100 ppm, respectively.

### 3 **3.2 Impact on spectral snow absorption coefficient and albedo**

4 Dust in snow effectively enhances the snow absorption coefficient, but its effect on the  
5 snow asymmetry factor and extinction efficiency is negligible (He et al., 2019).  
6 Therefore, we mainly focused on the effects of EDM and three cases of IDM (uniform,  
7 central, and peripheral) on the snow absorption coefficient ( $\sigma_{abs}$ ). Figure 4a displays the  
8  $\sigma_{abs}$  for EDM and IDM (uniform) as a function of wavelength at different dust  
9 concentrations. We used a snow grain radius of 200  $\mu\text{m}$  (Figure 4), which is comparable  
10 to previous observations of seasonal snow at mid to high latitudes in winter (Shi et al.,  
11 2020; Wang et al., 2017). The results showed that EDM and IDM have distinct impacts  
12 on  $\sigma_{abs}$  in UV and VIS, but small effects at wavelengths  $>1000$  nm, which is due to  
13 the optical properties of snow being affected by LAPs in UV and VIS and primarily  
14 affected by snow itself at wavelengths  $>1000$  nm. Additionally,  $\sigma_{abs}$  increased with  
15 increased dust mass concentrations. For instance,  $\sigma_{abs}$  increased from 0.007  $\text{m}^{-1}$  (pure  
16 snow) to 0.03, 0.14, and 1.37  $\text{m}^{-1}$  at 500 nm with 2, 10, and 100 ppm of dust with EDM,  
17 respectively. For IDM (uniform),  $\sigma_{abs}$  increased to 0.06, 0.28, and 2.80  $\text{m}^{-1}$  at 500 nm  
18 with 2, 10, and 100 ppm of dust, respectively, with corresponding enhancement factors  
19 of  $\sigma_{abs}$  ( $E_{\sigma_{abs}}$ , defined as the absorption coefficient of IDM divided by EDM) were  
20 1.84, 2.00, and 2.05. Furthermore, the  $\sigma_{abs}$  for two cases of non-uniform dust  
21 distribution in a spherical ice grain ( $r_{ef} = 200 \mu\text{m}$ ) depends on the wavelength, dust mass  
22 concentrations,  $\bar{r}_c$ , and  $\bar{r}_p$  (Figure 4b and 4c). We note that  $\bar{r}_c$  and  $\bar{r}_p$  values of 1  
23 correspond to uniformly distributed dust, and the  $\sigma_{abs}$  increases and decreases (with  
24 the decrease of  $\bar{r}_c$  and  $\bar{r}_p$ ) for IDM (central) and IDM (peripheral), respectively. For  
25 example,  $\sigma_{abs}$  increased by 29%, 32%, and 33% (500 nm) at dust mass concentrations  
26 of 2, 10, and 100 ppm, respectively, when  $\bar{r}_c$  decreased from 1 to 0.7 for IDM (central).  
27 However,  $\sigma_{abs}$  decreased by 41%, 44%, and 44% (500 nm) at dust mass concentrations  
28 of 2, 10, and 100 ppm, respectively, when  $\bar{r}_p$  decreased from 1 to 0.1 for IDM

1 (peripheral). This indicates that the IDM (central) further enhanced snowpack light  
2 absorption compared with the IDM (uniform), while the IDM (peripheral) reduced  
3 snowpack light absorption with a corresponding  $\sigma_{\text{abs}}$  between the value of  $\sigma_{\text{abs}}$  for  
4 IDM (uniform) and EDM. Figure 4d–f quantitatively shows the spectral snow  
5 absorption coefficient enhancement for IDM ( $E_{\sigma_{\text{abs}}}$ ). The enhancement decreased  
6 sharply with increasing wavelengths, then reduced to 1.0 (i.e., no enhancement) at  
7 wavelengths longer than  $\sim 1.0 \mu\text{m}$  because of strong dust absorption and weak snow  
8 absorption at shorter wavelengths. Obviously,  $E_{\sigma_{\text{abs}}}$  was affected by dust mass  
9 concentration,  $\bar{r}_c$ , and  $\bar{r}_p$ , but  $E_{\sigma_{\text{abs}}}$  was insensitive to dust mass concentration at  
10 wavelengths  $< 450 \text{ nm}$ .

11 Figure 5a–c shows the spectral snow albedo ( $\alpha_\lambda$ ) for EDM and IDM;  $\alpha_\lambda$  was  
12 consistent with  $\sigma_{\text{abs}}$ , with the effects mainly present at wavelengths  $< 1000 \text{ nm}$ .  
13 Generally,  $\alpha_\lambda$  decreased with increased dust mass concentrations in UV and VIS, and  
14 IDM was shown to further trigger the reduction of  $\alpha_\lambda$ . For example, for EDM  $\alpha_\lambda$  was  
15  $\sim 0.97, 0.95, 0.85$  (at  $500 \text{ nm}$ ) for dust concentrations of 2, 10, 100 ppm, respectively,  
16 which was higher than the values for IDM (uniform) ( $\sim 0.96, 0.93, 0.79$ , respectively).  
17 Compared with IDM (uniform), the  $\alpha_\lambda$  for IDM (central) decreased by 0.5%, 1.1%,  
18 and 3.5% (at  $500 \text{ nm}$ ) for dust concentrations of 2, 10, and 100 ppm, respectively, when  
19  $\bar{r}_c$  decreased from 1 to 0.7.  $\alpha_\lambda$  for IDM (peripheral) increased by 0.8%, 1.9%, and 6.2%  
20 (at  $500 \text{ nm}$ ) for the same dust concentrations, when  $\bar{r}_p$  decreased from 1 to 0.1.  
21 Moreover, the wavelength of the maximum  $\alpha_\lambda$  value varied from  $\sim 500 \text{ nm}$  to  $\sim 650 \text{ nm}$   
22 depending on the dust mass concentrations, which is consistent with changes of  $k_{\text{ef}}$ .  
23 Figure 5d–f shows the ratio ( $E_{\alpha_\lambda}$ ) of snow spectral albedo for IDM to EDM where we  
24 observed that the  $E_{\alpha_\lambda}$  increased with increasing wavelengths and dust concentrations,  
25 and then became stable at 1.0. This is because IDM can enhance the light absorption of  
26 snowpack more effectively at shorter wavelengths and higher dust concentrations  
27 (Figure 4). Additionally, the values of  $\bar{r}_c$  and  $\bar{r}_p$  also have non-negligible effects on  
28  $E_{\alpha_\lambda}$ , which can be decreased and increased with decreasing  $\bar{r}_c$  and  $\bar{r}_p$ , respectively.

1 We found that the optical properties of an ice grain containing uniformly distributed  
2 dust in its center, or concentric surface layer, can be affected by  $\bar{r}_c$  or  $\bar{r}_p$ . To better  
3 understand this effect, Figure 6a–b displays the  $\sigma_{\text{abs}}$  at 500 nm as a function of  $\bar{r}_c$  and  
4  $\bar{r}_p$  with different dust concentrations and  $r_{\text{ef}}$ . This demonstrates  $r_{\text{ef}}$  has negligible  
5 effects on  $\sigma_{\text{abs}}$  due to the geometric optical limits at  $r_{\text{ef}} \approx 50 \mu\text{m}$ , which shows the  
6 universal (independent of  $r_{\text{ef}}$ ) monotonic dependence of  $\sigma_{\text{abs}}$  on  $\bar{r}_c$  and  $\bar{r}_p$  for ice  
7 grains with  $r_{\text{ef}} \geq 50 \mu\text{m}$  (Velesco et al., 1997). As a result, the spectral absorption  
8 coefficient of snow containing polydispersed ice grains can be obtained using our  
9 results for a monodispersed model. Interestingly,  $\sigma_{\text{abs}}$  did not depend on  $\bar{r}_c$  when  $\bar{r}_c$   
10  $< 0.75$  and decreased almost linearly at higher  $\bar{r}_c$  values (Figure 6a); this phenomenon  
11 can be explained by geometric optical effects (Mackowski et al., 1990). However,  $\sigma_{\text{abs}}$   
12 was significantly affected by the dust mass concentration; for example,  $\sigma_{\text{abs}}$  at 500 nm  
13 was decreased by 28%, 32%, and 32% from its maximum value (0.08, 0.38, and 3.71  
14  $\text{m}^{-1}$ ) for dust concentrations of 2, 10, and 100 ppm, respectively, when  $\bar{r}_c$  increased  
15 from  $< 0.75$  to 1.0. The monotonic increase in  $\sigma_{\text{abs}}$  with the relative thickness of the  
16 polluted ice grain surface layer (i.e.,  $\bar{r}_p$ ) was also noteworthy (Figure 6b). The  
17 core/shell Mie theory calculations for ice grains with a thin surface layer ( $\bar{r}_p = 0.01$ )  
18 gave almost the same  $\sigma_{\text{abs}}$  as that obtained for the EDM. As a result, the  $\sigma_{\text{abs}}$   
19 increased rapidly with  $\bar{r}_p < 0.4$  and then increased more slowly until  $\bar{r}_p = 1$ , which  
20 corresponds to IDM (uniform).

21 The  $\alpha_\lambda$  at 500 nm as a function of  $\bar{r}_c$  and  $\bar{r}_p$  with different dust concentrations and  
22  $r_{\text{ef}}$ , is illustrated in Figure 6c and 6d. In general,  $\alpha_\lambda$  at 500 nm decreased with  
23 increasing dust mass concentration and  $r_{\text{ef}}$ ; the effect of grain radius can be explained  
24 by the fact that the snow extinction coefficient is inversely proportional to  $r_{\text{ef}}$ , so that  
25 for a given amount of dust, the single-scattering albedo of the snow-dust mixture is  
26 smaller for large snow grains (Gardner and Sharp, 2010). For a given dust mass  
27 concentration and  $r_{\text{ef}}$ , the  $\alpha_\lambda$  at 500 nm increased from its minimum value with  $\bar{r}_c$   
28  $< 0.75$  to the maximum value with  $\bar{r}_c = 1$ , corresponding to the findings of IDM

1 (uniform). For example, at dust concentrations of 2, 10, and 100 ppm, and a fixed  $r_{ef}$  of  
2 100  $\mu\text{m}$ , the  $\alpha_\lambda$  at 500 nm increased by 0.1%, 0.7%, and 2.6%, respectively, when  $\bar{r}_c$   
3 increased from  $<0.75$  to 1. When the  $r_{ef}$  was fixed at 500  $\mu\text{m}$ , the  $\alpha_\lambda$  at 500 nm  
4 increased by 0.8%, 1.9%, and 6.2% at dust concentrations of 2, 10, and 100 ppm,  
5 respectively. Conversely, the  $\alpha_\lambda$  at 500 nm decreased from its maximum value when  
6  $\bar{r}_p = 0.01$  (similar to EDM) to the minimum value with  $\bar{r}_p = 1$ , corresponding to the  
7 case of IDM (uniform). For example, the  $\alpha_\lambda$  at 500 nm decreased by 0.6%, 1.4%, and  
8 4.7% when  $\bar{r}_p$  increased from 0.01 to 1 for dust concentrations of 2, 10, and 100 ppm,  
9 respectively, and a fixed  $r_{ef}$  of 100  $\mu\text{m}$ , whereas for a  $r_{ef}$  of 500  $\mu\text{m}$ ,  $\alpha_\lambda$  decreased by  
10 1.4% (2 ppm dust), 3.3% (10 ppm), and 10.1% (100 ppm). These results indicate that  
11 dust mass concentrations and  $r_{ef}$  can amplify the influence of  $\bar{r}_c$  or  $\bar{r}_p$  on snow albedo.  
12 Moreover, the effect of dust mass concentration on snow albedo is similar to  $r_{ef}$ . For  
13 example, dust mass concentrations of 10 and 100 ppm and  $r_{ef}$  of 100 and 50  $\mu\text{m}$  gave  
14 similar  $\alpha_\lambda$  at 500 nm to dust mass concentrations of 2 and 10 ppm and  $r_{ef}$  of 500  $\mu\text{m}$ .  
15 According to this result, spectral albedo measurements at a single wavelength are  
16 insufficient to obtain the mass fraction of dust in snow cover because the same effect  
17 can also be explained by a combination of different ice grain sizes and a non-uniform  
18 distribution of dust inside the grains. It means that additional information is needed to  
19 determine accurate dust mass concentrations. This may be a set of measurements at  
20 various wavelengths in the VIS and NIR spectral ranges.

### 21 **3.3 Effects on broadband snow albedo**

22 Compared with the spectral optical properties, broadband results can provide more  
23 general knowledge for the relevant research community. Figure 7 shows the spectrally  
24 weighted  $\alpha_\lambda$  ( $\alpha_{\text{integrated}}$ ) over 300–2500 nm of a typical surface solar spectrum at mid  
25 to high latitudes, which is comparable with previous studies (Dang et al., 2017; Wang  
26 et al., 2017). Because the results of IDM (peripheral) effects on snow albedo fell  
27 between results from EDM and IDM (central), we do not consider the case of IDM  
28 (peripheral) in the following discussion. Instead, we focus on the effects of dust mass

1 concentration and  $r_{ef}$  on broadband snow albedo for EDM and IDM (uniform, central).  
2 Similar to  $\alpha_\lambda$ ,  $\alpha_{integrated}$  generally decreased with increasing dust mass  
3 concentrations and  $r_{ef}$  such that  $\alpha_{integrated}$  declined more for internal mixing than  
4 external mixing.  $\alpha_{integrated}$  showed ranges of 0.60–0.92, 0.54–0.92, and 0.51–0.92 for  
5 EDM, IDM (uniform), and IDM (central,  $\bar{r}_c < 0.75$ ), respectively, with dust mass  
6 concentrations of 0–100 ppm and  $r_{ef}$  of 50–1000  $\mu\text{m}$ . For a given dust mass  
7 concentration and  $r_{ef}$ ,  $\alpha_{integrated}$  for IDM (uniform) was smaller than EDM, which is  
8 due to higher light absorption in the UV and VIS bands for IDM (uniform) relative to  
9 EDM (Figure 4a). While  $\alpha_{integrated}$  for IDM (uniform) was larger compared with  
10 IDM (central,  $\bar{r}_c < 0.75$ ), this can be attributed to the fact that radiation is focused near  
11 the center of an ice grain with IDM (central) (Ackerman and Toon, 1981; Bohren, 1986),  
12 enabling further absorptions from inclusions near the center of a grain due to the lensing  
13 effect (Mackowski et al., 1990). For example,  $\alpha_{integrated}$  (dust concentration of 20  
14 ppm,  $r_{ef}$  of 500  $\mu\text{m}$ ) was 0.73 for IDM (uniform), less than EDM of 0.76, but higher  
15 than IDM (central,  $\bar{r}_c < 0.75$ ) of 0.72.

16 To quantify the effects of IDM on broadband snow albedo relative to EDM, we defined  
17 a broadband snow albedo scaling factor ( $E_{\alpha, integrated}$ ), which refers to the ratio of  
18  $\alpha_{integrated}$  of IDM to EDM. Generally, for dust mass concentrations from 0 to 100 ppm  
19 and  $r_{ef}$  of 50–1000  $\mu\text{m}$ ,  $E_{\alpha, integrated}$  varied from 0.89 to  $\sim 1.00$  for IDM (uniform) (Figure  
20 8a) and from 0.85 to  $\sim 1.00$  for IDM (central,  $\bar{r}_c < 0.75$ ) (Figure 8b).  $E_{\alpha, integrated}$   
21 decreased significantly with increasing dust mass concentration and  $r_{ef}$ . In addition,  $E_{\alpha, integrated}$   
22 for IDM (central,  $\bar{r}_c < 0.75$ ) was smaller than IDM (uniform). These results  
23 have implications for the effects of IDM in real environments. For example, IMC has  
24 typical dust concentrations of  $\sim 10$  ppm (Wang et al., 2013), so  $E_{\alpha, integrated}$  ( $r_{ef}$  of 50–  
25 1000  $\mu\text{m}$ ) was 0.96–0.99 and 0.95–0.99 for IDM (uniform) and IDM (central,  $\bar{r}_c <$   
26 0.75), respectively. In contrast, dust concentrations are typically  $\sim 100$  ppm in the TP  
27 (Ming et al., 2016; Li et al., 2017, 2018), so  $E_{\alpha, integrated}$  ranged from 0.89 to 0.98 and  
28 0.85 to 0.96 for IDM (uniform) and IDM (central,  $\bar{r}_c < 0.75$ ), respectively. The results

1 show that IDM (uniform) and IDM (central,  $\bar{r}_c < 0.75$ ) reduced broadband snow  
2 albedo by  $\sim 2.5\%$  and  $\sim 3.0\%$ , respectively, in clean snow and  $\sim 6.5\%$  and  $\sim 9.5\%$ ,  
3 respectively, in polluted snow relative to EDM. Moreover, the sensitivity of  $E_{\alpha, \text{integrated}}$   
4 to mineral dust decreased with increasing dust concentrations. For example, the  
5 difference in  $E_{\alpha, \text{integrated}}$  ( $r_{ef}$  of  $500 \mu\text{m}$ ) between dust concentrations of 10 and 20 ppm  
6 was 0.011 and 0.015 for IDM (uniform) and IDM (central,  $\bar{r}_c < 0.75$ ), respectively,  
7 while the corresponding differences between dust concentrations of 90 and 100 ppm  
8 were only 0.004 and 0.005. These results provide a convenient method to calculate the  
9 albedo of IDM when the albedo of EDM has been obtained for a given dust mass  
10 concentration and  $r_{ef}$ .

### 11 **3.4 Uncertainties**

12 Although we calculated the imaginary RI values of dust using previous studies (section  
13 2.2), there are still large variations which strongly depend on dust composition (e.g.,  
14 hematite/iron content) (Balkanski et al., 2007; Wagner et al., 2012). To roughly account  
15 for this, we estimated the influence of chosen imaginary RI values on spectrally  
16 weighted snow albedo ( $E_{\alpha, \text{integrated}}$ ) by increasing and decreasing the calculated  
17 imaginary RI values by 50%. These changes in imaginary RIs are plausible because  
18 they are consistent with other studies (McConnell et al., 2010; Wagner et al., 2012).  
19 The results showed that  $E_{\alpha, \text{integrated}}$  uncertainties attributed to the imaginary RIs of dust  
20 were  $\pm 3.9\%$  and  $\pm 5.2\%$  for IDM (uniform) and IDM (central,  $\bar{r}_c < 0.75$ ), respectively.  
21 In contrast, observations have displayed large variations in the size distribution of dust  
22 in the atmosphere and snow, and this variation is strongly affected by the dust source  
23 and transport (Mahowald et al., 2014; Shao et al., 2011). In our standard simulation, we  
24 assumed a log-normal dust size distribution with a geometric mean diameter of  $0.65 \mu\text{m}$   
25 and a standard deviation of 2.0 (equivalent to an effective radius of  $1.1 \mu\text{m}$ ), which  
26 is typical for dust transported long-range (Formenti et al., 2011; Maring et al., 2003);  
27 nearer sources of dust tend to be larger (Kok, 2011). Therefore, we investigated the  
28 effects of dust particle size on our results by assuming another two log-normal size



1 distributions with effective radii of 2.5  $\mu\text{m}$  and 5.0  $\mu\text{m}$ , which were within the observed  
2 size ranges in the atmosphere and snow and comparable with previously analyzed dust  
3 particle sizes (Maring et al., 2003; Shao and Mao, 2016; Zhang et al., 2003). The results  
4 showed that the uncertainty of  $E_{\alpha, \text{integrated}}$  attributed to dust diameter was  $\pm 6.1\%$  for both  
5 IDM (uniform) and IDM (central,  $\bar{r}_c < 0.75$ ), but it should be emphasized that this  
6 uncertainty estimate accounts only for the impact of dust size on snow albedo in the  
7 case of external mixing, since the impact on albedo due to dust size cannot be evaluated  
8 when using the effective medium approximation. Overall, the total uncertainty of  $E_{\alpha, \text{integrated}}$   
9 from variations of imaginary RIs and dust diameter was  $\pm 11.0\%$  and  $\pm 11.2\%$  for  
10 IDM (uniform) and IDM (central,  $\bar{r}_c < 0.75$ ), respectively, with dust mass  
11 concentrations of 0–100 ppm and  $r_{ef}$  of 50–1000  $\mu\text{m}$ . Specifically, the uncertainty  
12 increased with increasing  $r_{ef}$  and dust concentrations.

### 13 **3.5 Measurement-based estimate of the effects of dust on snow albedo**

14 Finally, widespread dust concentrations in snow across the Northern Hemisphere were  
15 obtained to assess the effects of dust on snow albedo in real snowpack. Figure 9 shows  
16 measured dust concentrations in snow in different regions; dust concentrations spanned  
17 a broad range of values because of spatial and temporal variations in emissions,  
18 transportation, and deposition among the different regions. Dust concentrations widely  
19 varied from  $\sim 3$  ppm to  $\sim 600$  ppm, with the highest concentration in NAM and lowest  
20 in the EP (Di Mauro et al., 2015; Lim et al., 2014; Painter et al., 2012; Reynolds et al.,  
21 2020). However, snow samples collected in the days after a significant dust transport  
22 event showed that dust concentrations in snow can be up to  $\sim 70$  ppm in the EP (Di  
23 Mauro et al., 2015). Additionally, the average dust concentrations in fresh snow were  
24 18, 6, and 28 ppm in the southern TP, central TP, and northern TP, respectively, similar  
25 to the IMC (12 ppm) (Wang et al., 2013). However, dust concentrations in aged snow  
26 (120, 300, and 140 ppm) were one to two orders of magnitude higher than in fresh snow,  
27 indicating the important correlation between snow type and dust concentration (Zhang  
28 et al., 2017, 2018).

1 We calculated the broadband snow albedo for EDM, IDM (uniform), and IDM (central,  
2  $\bar{r}_c < 0.75$ ) based on the measured dust concentrations (Figure 10). The results showed  
3 that broadband snow albedo decreased by 0.8%, 1.4%, and 1.6% in the EP for EDM,  
4 IDM (uniform), and IDM (central,  $\bar{r}_c < 0.75$ ), respectively, which was similar to SJ.  
5 However, the broadband snow albedo decreased by up to 5.6%, 8.1%, and 9.4% in the  
6 EP after a significant dust transport event, indicating strong snow albedo reduction  
7 during these events. In addition, broadband snow albedo was reduced by 2.0%, 3.1%,  
8 and 3.6% in IMC for EDM, IDM (uniform), and IDM (central,  $\bar{r}_c < 0.75$ ), respectively.  
9 Similar results were also found for the southern TP, central TP, and northern TP where  
10 the broadband snow albedo for fresh snow was reduced by 2.5%, 1.4%, and 3.3%,  
11 respectively, for EDM, 3.9%, 2.1%, and 5.1% for IDM (uniform), and 4.5%, 2.4%, and  
12 5.7% for IDM (central,  $\bar{r}_c < 0.75$ ). However, the broadband snow albedo was more  
13 significantly reduced for aged snow: up to 6.0%, 8.1%, and 7.5% for EDM, 9.5%,  
14 11.6%, and 10.5% for IDM (uniform), and 10.9%, 13.2%, and 12.3% for IDM (central,  
15  $\bar{r}_c < 0.75$ ) in the southern, central, and northern TP, respectively. This indicates that the  
16 effects of dust on snow albedo showed stronger reductions during snowmelt periods, it  
17 is worth noting that the effect of dust on snow albedo for aged snow could be  
18 underestimated due to the larger snow grain effective radius ( $r_{ef}$ ) than fresh snow.  
19 Moreover, the largest broadband snow albedo reductions were found in NAM with  
20 ranges of 9.8%–17.6%, 13.9%–24.1%, and 15.9%–27.0% for EDM, IDM (uniform),  
21 and IDM (central,  $\bar{r}_c < 0.75$ ), respectively. These results suggest that the effects of  
22 external or internal dust–snow mixing on snow albedo are particularly significant for  
23 the TP and NAM regions, with stronger reductions in albedo. Therefore, these results  
24 can have significant impacts on both local hydrological cycles and regional climate  
25 change (Oaida et al., 2015; Xie et al., 2018).

#### 26 **4. Discussion**

27 In this study, the application of the effective medium approximation greatly simplifies  
28 the complexity of snow radiation transfer calculation for dust–snow internal mixing,

1 and the effect of non-uniform distribution of dust in snow grains on snowpack optical  
2 properties are explicitly quantified for the first time. However, it is worth noting that  
3 this method has its limitation when applying to large particles (e.g., dust) in snow  
4 (Bohren 1986; Flanner et al., 2012), which can create some errors for the albedo  
5 calculation of dust–snow internal mixing. To verify the credibility of our results, we  
6 carefully make a comparison with the more rigorous calculations found in He et al.  
7 (2019), which used the geometric-optics surface-wave approach (GOS) to consider the  
8 impact of dust–snow uniform internal mixing on snow albedo reduction. As shown in  
9 Figure 11, the results show that the enhancement ratio of snow albedo reduction (1.28)  
10 due to dust–snow internal mixing (relative to external mixing) is slightly higher than  
11 the value (1.16) reported by He et al. (2019), and this deviation is comparable to that  
12 caused by snow nonsphericity (He et al., 2019). Therefore, we indicated that the  
13 effective medium approximation used in this study is reasonable and reliable.

14 Over the past few decades, the effects of dust in snow on reductions in albedo have  
15 been widely demonstrated (Skiles et al., 2018; Zhang et al., 2018). However, the  
16 magnitude of these effects has only been studied in a few regions, and uncertainties still  
17 remain. Our study indicates that the albedo of dust-contaminated snowpack can be  
18 affected by the dust–ice mixing state. In particular, IDM enhanced light absorption and  
19 reduced snow albedo more significantly compared with EDM. For example, in IMC  
20 and the TP, IDM reduced snow albedo by ~5% relative to EDM at a typical dust mass  
21 concentration of 20 ppm and a snow grain radius of 500  $\mu\text{m}$ . This exceeds the  
22 contribution of BC to snow light absorption over most areas of North America and the  
23 Arctic (Dang et al., 2017). In addition, the effects of IDM on snow albedo were  
24 amplified by higher dust mass concentrations and larger snow grain sizes. We therefore  
25 strongly suggest that IDM must be considered in future climate models, particularly to  
26 more accurately evaluate the climate in areas where snowpack is heavily contaminated  
27 with dust and is experiencing melting.

28 The mixed state between dust and snow gradually progresses from partial external

1 mixing to wholly internally mixed. Therefore, assuming a completely external mixing  
2 of dust and snow grains will underestimate the effects of dust on snow albedo and  
3 radiative forcing in numerical models (e.g., Dang et al., 2015; Nagorski et al., 2019).  
4 Similarly, assuming completely internal mixing of dust and snow grains will  
5 overestimate the effects of dust (e.g., He et al., 2019; Liou et al., 2014). Zhao et al.  
6 (2014) underestimated the effects of dust by treating wet-deposited dust as externally  
7 mixed with snow grains. In future studies, we recommend the actual ratio between  
8 external and internal mixing for dust in snow be examined with an environmental  
9 scanning electron microscope equipped with a cold stage.

## 10 **5. Conclusions**

11 In this study, the effects of dust particles on absorption coefficients and snow albedo  
12 were theoretically analyzed by combining asymptotic radiative transfer theory and  
13 (core/shell) Mie theory. We initially considered external mixing – when dust is present  
14 between ice grains – and variations of internal mixing of dust within ice grains. We  
15 found that snow spectral absorption coefficients of IDM were larger than EDM across  
16 UV to NIR wavelengths, but were negligible at wavelengths >1000 nm. The absorption  
17 enhancement (relative to EDM) was wavelength-dependent and increased with  
18 increased dust concentrations.

19 Compared with a uniform distribution of dust particles in ice grains, our calculations  
20 showed that non-uniformly distributed dust particles may lead to significantly different  
21 snow spectral absorption coefficients in the VIS band. Snow spectral absorption  
22 coefficients were further increased when all of the dust was positioned in the central  
23 part of ice grains, while the maximum absorption coefficient was found when the radius  
24 of a dust-polluted core was <75% of the ice grain radius. In contrast, snow spectral  
25 absorption coefficients decreased when all of the dust was positioned in the surface  
26 layer of ice grains, and the minimum absorption coefficient was observed in the thin  
27 surface layer of dust-polluted ice grains, which was similar for EDM. As a result,  
28 broadband snow albedo decreased by up to 21%, 30%, and 33% for EDM, IDM

1 (uniform), and IDM (central,  $\bar{r}_c < 0.75$ ), respectively, at dust concentrations of 100  
2 ppm and  $r_{ef}$  of 1000  $\mu\text{m}$ .

3 Based on comprehensive field measurements across the Northern Hemisphere, the  
4 effect of dust on snow albedo in real snowpack was evaluated by assuming external and  
5 internal dust–snow mixing. The largest reductions in broadband snow albedo were in  
6 NAM because that region had the highest average dust concentrations; IDM (uniform)  
7 and IDM (central,  $\bar{r}_c < 0.75$ ) further decreased snow albedo by 4.6%–7.8% and 6.8%–  
8 11.4%, respectively, compared with EDM. This implies an important influence of  
9 internal dust–snow mixing in NAM.

### 10 **Data availability**

11 The code of (core/shell) Mie theory used in this study can be found at [http://gwest.gats-](http://gwest.gats-inc.com/software/software_page.html)  
12 [inc.com/software/software\\_page.html](http://gwest.gats-inc.com/software/software_page.html).

### 13 **Author contributions**

14 WX designed the study and evolved the overarching research goals and aims. STL  
15 wrote the first draft with contributions from all co-authors. STL and CJC applied formal  
16 techniques such as statistical, mathematical, and computational to analyze study data.  
17 CY and XXY collected the dust measurements across the Northern Hemisphere. ZY  
18 and PW provided the majority of the methodology and software. CQL and ZXL  
19 provided technical guidance. All authors contributed to the improvement of results and  
20 revised the final paper.

### 21 **Competing interests**

22 The authors declare that they have no conflict of interest.

### 23 **Acknowledgments**

24 This work was supported by the National Science Fund for Distinguished Young  
25 Scholars (42025102), the National Key Research and Development Program of China  
26 (grant number 2019YFA0606801), and the National Natural Science Foundation of

1 China (grant number 41975157, 41775144 and 42075061).

2

## 1 **References**

- 2 Aoki, T., Aoki, T., Fukabori, M., Hachikubo, A., Tachibana, Y., and Nishio, F.: Effects  
3 of snow physical parameters on spectral albedo and bidirectional reflectance of snow  
4 surface, *J Geophys Res-Atmos*, 105, 10219-10236, 10.1029/1999jd901122, 2000.
- 5 Balkanski, Y., Schulz, M., Claquin, T., and Guibert, S.: Reevaluation of Mineral aerosol  
6 radiative forcings suggests a better agreement with satellite and AERONET data, *Atmos.*  
7 *Chem. Phys.*, 7, 81-95, 10.5194/acp-7-81-2007, 2007.
- 8 Bohren, C. F.: Applicability of Effective-Medium Theories to Problems of Scattering  
9 and Absorption by Nonhomogeneous Atmospheric Particles, *J Atmos Sci*, 43, 468-475,  
10 10.1175/1520-0469(1986)043<0468:Aoemtt>2.0.Co;2, 1986.
- 11 Casey, K. A., Kaspari, S. D., Skiles, S. M., Kreutz, K., and Handley, M. J.: The spectral  
12 and chemical measurement of pollutants on snow near South Pole, Antarctica, *J*  
13 *Geophys Res-Atmos*, 122, 6592-6610, 10.1002/2016jd026418, 2017.
- 14 Creamean, J. M., Suski, K. J., Rosenfeld, D., Cazorla, A., DeMott, P. J., Sullivan, R. C.,  
15 White, A. B., Ralph, F. M., Minnis, P., Comstock, J. M., Tomlinson, J. M., and Prather,  
16 K. A.: Dust and Biological Aerosols from the Sahara and Asia Influence Precipitation  
17 in the Western U.S., *Science*, 339, 1572-1578, 10.1126/science.1227279, 2013.
- 18 Dang, C., Brandt, R. E., and Warren, S. G.: Parameterizations for narrowband and  
19 broadband albedo of pure snow and snow containing mineral dust and black carbon, *J*  
20 *Geophys Res-Atmos*, 120, 5446-5468, 10.1002/2014JD022646, 2015.
- 21 Dang, C., Fu, Q., and Warren, S. G.: Effect of Snow Grain Shape on Snow Albedo, *J*  
22 *Atmos Sci*, 73, 3573-3583, 10.1175/JAS-D-15-0276.1, 2016.
- 23 Dang, C., Warren, S. G., Fu, Q., Doherty, S. J., Sturm, M., and Su, J.: Measurements of  
24 light-absorbing particles in snow across the Arctic, North America, and China: Effects  
25 on surface albedo, *J Geophys Res-Atmos*, 122, 10149-10168, 10.1002/2017jd027070,  
26 2017.
- 27 DeMott, P. J., Prenni, A. J., Liu, X., Kreidenweis, S. M., Petters, M. D., Twohy, C. H.,  
28 Richardson, M. S., Eidhammer, T., and Rogers, D. C.: Predicting global atmospheric

1 ice nuclei distributions and their impacts on climate, *P Natl Acad Sci USA*, 107, 11217-  
2 11222, 10.1073/pnas.0910818107, 2010.

3 Di Mauro, B., Fava, F., Ferrero, L., Garzonio, R., Baccolo, G., Delmonte, B., and  
4 Colombo, R.: Mineral dust impact on snow radiative properties in the European Alps  
5 combining ground, UAV, and satellite observations, *J Geophys Res-Atmos*, 120, 6080-  
6 6097, 10.1002/2015jd023287, 2015.

7 Di Mauro, B., Garzonio, R., Baccolo, G., Franzetti, A., Pittino, F., Leoni, B., Remias,  
8 D., Colombo, R., and Rossini, M.: Glacier algae foster ice-albedo feedback in the  
9 European Alps, *Sci Rep-Uk*, 10, 4739, 10.1038/s41598-020-61762-0, 2020.

10 Dombrovsky L. A., and Baillis D.: Thermal radiation in disperse systems: an  
11 engineering approach. New York: Begell House, 2010.

12 Dombrovsky, L. A., and Kokhanovsky, A. A.: Light absorption by polluted snow cover:  
13 Internal versus external mixture of soot, *Journal of Quantitative Spectroscopy and*  
14 *Radiative Transfer*, 242, 106799, 10.1016/j.jqsrt.2019.106799, 2020.

15 Flanner, M. G., Zender, C. S., Randerson, J. T., and Rasch, P. J.: Present-day climate  
16 forcing and response from black carbon in snow, *Journal of Geophysical Research*, 112,  
17 10.1029/2006jd008003, 2007.

18 Flanner, M. G., Shell, K. M., Barlage, M., Perovich, D. K., and Tschudi, M. A.:  
19 Radiative forcing and albedo feedback from the Northern Hemisphere cryosphere  
20 between 1979 and 2008, *Nat Geosci*, 4, 151-155, 10.1038/ngeo1062, 2011.

21 Flanner, M. G., Liu, X., Zhou, C., Penner, J. E., and Jiao, C.: Enhanced solar energy  
22 absorption by internally-mixed black carbon in snow grains, *Atmos Chem Phys*, 12,  
23 4699-4721, 10.5194/acp-12-4699-2012, 2012.

24 Formenti, P., Schutz, L., Balkanski, Y., Desboeufs, K., Ebert, M., Kandler, K., Petzold,  
25 A., Scheuven, D., Weinbruch, S., and Zhang, D.: Recent progress in understanding  
26 physical and chemical properties of African and Asian mineral dust, *Atmos Chem Phys*,  
27 11, 8231-8256, 10.5194/acp-11-8231-2011, 2011.

28 France, J. L., Reay, H. J., King, M. D., Voisin, D., Jacobi, H. W., Domine, F., Beine, H.,



1 Anastasio, C., MacArthur, A., and Lee-Taylor, J.: Hydroxyl radical and NO<sub>x</sub> production  
2 rates, black carbon concentrations and light-absorbing impurities in snow from field  
3 measurements of light penetration and nadir reflectivity of onshore and offshore coastal  
4 Alaskan snow, *J Geophys Res-Atmos*, 117, 10.1029/2011jd016639, 2012.

5 Gabbi, J., Huss, M., Bauder, A., Cao, F., and Schwikowski, M.: The impact of Saharan  
6 dust and black carbon on albedo and long-term mass balance of an Alpine glacier,  
7 *Cryosphere*, 9, 1385-1400, 10.5194/tc-9-1385-2015, 2015.

8 Gardner, A. S., and Sharp, M. J.: A review of snow and ice albedo and the development  
9 of a new physically based broadband albedo parameterization, *Journal of Geophysical*  
10 *Research*, 115, 10.1029/2009jf001444, 2010.

11 Grenfell, T. C., Light, B., and Sturm, M.: Spatial distribution and radiative effects of  
12 soot in the snow and sea ice during the SHEBA experiment, *J Geophys Res-Oceans*,  
13 107, 10.1029/2000jc000414, 2002.

14 Hadley, O. L., and Kirchstetter, T. W.: Black-carbon reduction of snow albedo, *Nat Clim*  
15 *Change*, 2, 437-440, 10.1038/nclimate1433, 2012.

16 Hansen, J., and Nazarenko, L.: Soot climate forcing via snow and ice albedos, *P Natl*  
17 *Acad Sci USA*, 101, 423-428, 10.1073/pnas.2237157100, 2004.

18 He, C., Liou, K.-N., Takano, Y., Chen, F., and Barlage, M.: Enhanced Snow Absorption  
19 and Albedo Reduction by Dust-Snow Internal Mixing: Modeling and Parameterization,  
20 *J Adv Model Earth Sy*, n/a, 10.1029/2019ms001737, 2019.

21 He, C. L., Flanner, M. G., Chen, F., Barlage, M., Liou, K. N., Kang, S. C., Ming, J., and  
22 Qian, Y.: Black carbon-induced snow albedo reduction over the Tibetan Plateau:  
23 uncertainties from snow grain shape and aerosol-snow mixing state based on an updated  
24 SNICAR model, *Atmos Chem Phys*, 18, 11507-11527, 10.5194/acp-18-11507-2018,  
25 2018.

26 Horhold, M. W., Laepple, T., Freitag, J., Bigler, M., Fischer, H., and Kipfstuhl, S.: On  
27 the impact of impurities on the densification of polar firn, *Earth Planet Sc Lett*, 325, 93-  
28 99, 10.1016/j.epsl.2011.12.022, 2012.

1 Huang, J. P., Wang, T. H., Wang, W. C., Li, Z. Q., and Yan, H. R.: Climate effects of  
2 dust aerosols over East Asian arid and semiarid regions, *J Geophys Res-Atmos*, 119,  
3 11398-11416, 10.1002/2014JD021796, 2014.

4 Jacobson, M. Z.: Climate response of fossil fuel and biofuel soot, accounting for soot's  
5 feedback to snow and sea ice albedo and emissivity, *J Geophys Res-Atmos*, 109,  
6 10.1029/2004jd004945, 2004.

7 Kaspari, S., Skiles, S. M., Delaney, I., Dixon, D., and Painter, T. H.: Accelerated glacier  
8 melt on Snow Dome, Mount Olympus, Washington, USA, due to deposition of black  
9 carbon and mineral dust from wildfire, *J Geophys Res-Atmos*, 120, 2793-2807,  
10 10.1002/2014jd022676, 2015.

11 Kok, J. F.: A scaling theory for the size distribution of emitted dust aerosols suggests  
12 climate models underestimate the size of the global dust cycle, *P Natl Acad Sci USA*,  
13 108, 1016-1021, 10.1073/pnas.1014798108, 2011.

14 Kokhanovsky, A.: Spectral reflectance of solar light from dirty snow: a simple  
15 theoretical model and its validation, *Cryosphere*, 7, 1325-1331, 10.5194/tc-7-1325-  
16 2013, 2013.

17 Kokhanovsky, A. A., and Zege, E. P.: Scattering optics of snow, *Appl Optics*, 43, 1589-  
18 1602, 10.1364/AO.43.001589, 2004.

19 Koledintseva, M. Y., DuBroff, R. E., and Schwartz, R. W.: Maxwell Garnett Rule for  
20 Dielectric Mixtures with Statistically Distributed Orientations of Inclusions, *Prog*  
21 *Electromagn Res*, 99, 131-148, 10.2528/PIER09091605, 2009.

22 Kuchiki, K., Aoki, T., Niwano, M., Matoba, S., Kodama, Y., and Adachi, K.: Elemental  
23 carbon, organic carbon, and dust concentrations in snow measured with thermal optical  
24 and gravimetric methods: Variations during the 2007-2013 winters at Sapporo, Japan,  
25 *J Geophys Res-Atmos*, 120, 868-882, 10.1002/2014JD022144, 2015.

26 Li, X. F., Kang, S. C., He, X. B., Qu, B., Tripathee, L., Jing, Z. F., Paudyal, R., Li, Y.,  
27 Zhang, Y. L., Yan, F. P., Li, G., and Li, C. L.: Light-absorbing impurities accelerate  
28 glacier melt in the Central Tibetan Plateau, *Sci Total Environ*, 587, 482-490,

1 10.1016/j.scitotenv.2017.02.169, 2017.

2 Li, X. F., Kang, S. C., Zhang, G. S., Qu, B., Tripathee, L., Paudyal, R., Jing, Z. F., Zhang,  
3 Y. L., Yan, F. P., Li, G., Cui, X. Q., Xu, R., Hu, Z. F., and Li, C. L.: Light-absorbing  
4 impurities in a southern Tibetan Plateau glacier: Variations and potential impact on  
5 snow albedo and radiative forcing, *Atmos Res*, 200, 77-87,  
6 10.1016/j.atmosres.2017.10.002, 2018.

7 Li, Y., Chen, J., Kang, S., Li, C., Qu, B., Tripathee, L., Yan, F., Zhang, Y., Guo, J., Gul,  
8 C., and Qin, X.: Impacts of black carbon and mineral dust on radiative forcing and  
9 glacier melting during summer in the Qilian Mountains, northeastern Tibetan Plateau,  
10 *The Cryosphere Discuss.*, 2016, 1-14, 10.5194/tc-2016-32, 2016.

11 Li, Y., Kang, S., Chen, J., Hu, Z., Wang, K., Paudyal, R., Liu, J., Wang, X., Qin, X., and  
12 Sillanpää, M.: Black carbon in a glacier and snow cover on the northeastern Tibetan  
13 Plateau: Concentrations, radiative forcing and potential source from local topsoil, *Sci*  
14 *Total Environ*, 10.1016/j.scitotenv.2019.05.469, 2019.

15 Libois, Q., Picard, G., France, J. L., Arnaud, L., Dumont, M., Carmagnola, C. M., and  
16 King, M. D.: Influence of grain shape on light penetration in snow, *Cryosphere*, 7, 1803-  
17 1818, 10.5194/tc-7-1803-2013, 2013.

18 Lim, S., Fain, X., Zanatta, M., Cozic, J., Jaffrezo, J. L., Ginot, P., and Laj, P.: Refractory  
19 black carbon mass concentrations in snow and ice: method evaluation and inter-  
20 comparison with elemental carbon measurement, *Atmospheric Measurement*  
21 *Techniques*, 7, 3307-3324, 10.5194/amt-7-3307-2014, 2014.

22 Liou, K. N., Takano, Y., and Yang, P.: Light absorption and scattering by aggregates:  
23 Application to black carbon and snow grains, *J Quant Spectrosc Ra*, 112, 1581-1594,  
24 10.1016/j.jqsrt.2011.03.007, 2011.

25 Liou, K. N., Takano, Y., He, C., Yang, P., Leung, L. R., Gu, Y., and Lee, W. L.:  
26 Stochastic parameterization for light absorption by internally mixed BC/dust in snow  
27 grains for application to climate models, *J Geophys Res-Atmos*, 119, 7616-7632,  
28 10.1002/2014jd021665, 2014.

1 Mackowski, D. W., Altenkirch, R. A., and Menguc, M. P.: Internal Absorption Cross-  
2 Sections in a Stratified Sphere, *Appl Optics*, 29, 1551-1559, 10.1364/AO.29.001551,  
3 1990.

4 Mahowald, N., Albani, S., Kok, J. F., Engelstaeder, S., Scanza, R., Ward, D. S., and  
5 Flanner, M. G.: The size distribution of desert dust aerosols and its impact on the Earth  
6 system, *Aeolian Res*, 15, 53-71, 10.1016/j.aeolia.2013.09.002, 2014.

7 Maring, H., Savoie, D. L., Izaguirre, M. A., Custals, L., and Reid, J. S.: Mineral dust  
8 aerosol size distribution change during atmospheric transport, *J Geophys Res-Atmos*,  
9 108, 10.1029/2002JD002536, 2003.

10 Markel, V. A.: Introduction to the Maxwell Garnett approximation: tutorial, *J Opt Soc*  
11 *Am A*, 33, 1244-1256, 10.1364/JOSAA.33.001244, 2016.

12 Marley, N. A., Gaffney, J. S., Baird, C., Blazer, C. A., Drayton, P. J., and Frederick, J.  
13 E.: An empirical method for the determination of the complex refractive index of size-  
14 fractionated atmospheric aerosols for radiative transfer calculations, *Aerosol Sci Tech*,  
15 34, 535-549, 10.1080/02786820118599, 2001.

16 Matt, F. N., Burkhart, J. F., and Pietikäinen, J. P.: Modelling hydrologic impacts of light  
17 absorbing aerosol deposition on snow at the catchment scale, *Hydrol. Earth Syst. Sci.*,  
18 22, 179-201, 10.5194/hess-22-179-2018, 2018.

19 Maxwell-Garnett, J. C., and Larmor, J.: XII. Colours in metal glasses and in metallic  
20 films, *Philosophical Transactions of the Royal Society of London. Series A, Containing*  
21 *Papers of a Mathematical or Physical Character*, 203, 385-420, 10.1098/rsta.1904.0024,  
22 1904.

23 McConnell, C. L., Formenti, P., Highwood, E. J., and Harrison, M. A. J.: Using aircraft  
24 measurements to determine the refractive index of Saharan dust during the DODO  
25 Experiments, *Atmos Chem Phys*, 10, 3081-3098, 10.5194/acp-10-3081-2010, 2010.

26 Ming, J., Xiao, C. D., Wang, F. T., Li, Z. Q., and Li, Y. M.: Grey Tienshan Urumqi  
27 Glacier No.1 and light-absorbing impurities, *Environ Sci Pollut R*, 23, 9549-9558,  
28 10.1007/s11356-016-6182-7, 2016.

1 Nagorski, S. A., Kaspari, S. D., Hood, E., Fellman, J. B., and Skiles, S. M. J. J. o. G. R.  
2 A.: Radiative Forcing by Dust and Black Carbon on the Juneau Icefield, Alaska,  
3 10.1029/2018JD029411, 2019.

4 Niu, H. W., Kang, S. C., Zhang, Y. L., Shi, X. Y., Shi, X. F., Wang, S. J., Li, G., Yan, X.  
5 G., Pu, T., and He, Y. Q.: Distribution of light-absorbing impurities in snow of glacier  
6 on Mt. Yulong, southeastern Tibetan Plateau, Atmos Res, 197, 474-484,  
7 10.1016/j.atmosres.2017.07.004, 2017.

8 Niwano, M., Aoki, T., Kuchiki, K., Hosaka, M., and Kodama, Y.: Snow Metamorphism  
9 and Albedo Process (SMAP) model for climate studies: Model validation using  
10 meteorological and snow impurity data measured at Sapporo, Japan, J Geophys Res-  
11 Earth, 117, -, 10.1029/2011jf002239, 2012.

12 Oaida, C. M., Xue, Y. K., Flanner, M. G., Skiles, S. M., De Sales, F., and Painter, T. H.:  
13 Improving snow albedo processes in WRF/SSiB regional climate model to assess  
14 impact of dust and black carbon in snow on surface energy balance and hydrology over  
15 western US, J Geophys Res-Atmos, 120, 3228-3248, 10.1002/2014JD022444, 2015.

16 Painter, T. H., Skiles, S. M., Deems, J. S., Bryant, A. C., and Landry, C. C.: Dust  
17 radiative forcing in snow of the Upper Colorado River Basin: 1. A 6 year record of  
18 energy balance, radiation, and dust concentrations, Water Resour Res, 48,  
19 10.1029/2012WR011985, 2012.

20 Pu, W., Cui, J., Shi, T., Zhang, X., He, C., and Wang, X.: The remote sensing of radiative  
21 forcing by light-absorbing particles (LAPs) in seasonal snow over northeastern China,  
22 Atmos. Chem. Phys., 19, 9949-9968, 10.5194/acp-19-9949-2019, 2019.

23 Qian, Y., Yasunari, T. J., Doherty, S. J., Flanner, M. G., Lau, W. K. M., Ming, J., Wang,  
24 H. L., Wang, M., Warren, S. G., and Zhang, R. D.: Light-absorbing Particles in Snow  
25 and Ice: Measurement and Modeling of Climatic and Hydrological impact, Advances  
26 in Atmospheric Sciences, 32, 64-91, 10.1007/s00376-014-0010-0, 2015.

27 Qu, B., Ming, J., Kang, S. C., Zhang, G. S., Li, Y. W., Li, C. D., Zhao, S. Y., Ji, Z. M.,  
28 and Cao, J. J.: The decreasing albedo of the Zhadang glacier on western

1 Nyainqentanglha and the role of light-absorbing impurities, *Atmos Chem Phys*, 14,  
2 11117-11128, 10.5194/acp-14-11117-2014, 2014.

3 Rahimi, S., Liu, X., Wu, C., Lau, W. K., Brown, H., Wu, M., and Qian, Y.: Quantifying  
4 snow darkening and atmospheric radiative effects of black carbon and dust on the South  
5 Asian monsoon and hydrological cycle: experiments using variable-resolution CESM,  
6 *Atmos. Chem. Phys.*, 19, 12025-12049, 10.5194/acp-19-12025-2019, 2019.

7 Rango, A., Wergin, W. P., and Erbe, E. F.: Snow crystal imaging using scanning electron  
8 microscopy .2. Metamorphosed snow, *Hydrolog Sci J*, 41, 235-250,  
9 10.1080/02626669609491495, 1996.

10 Reay, H. J., France, J. L., and King, M. D.: Decreased albedo, e-folding depth and  
11 photolytic OH radical and NO<sub>2</sub> production with increasing black carbon content in  
12 Arctic snow, *J Geophys Res-Atmos*, 117, 10.1029/2011jd016630, 2012.

13 Reynolds, R. L., Goldstein, H. L., Moskowitz, B. M., Kokaly, R. F., Munson, S. M.,  
14 Solheid, P., Breit, G. N., Lawrence, C. R., and Derry, J.: Dust deposited on snow cover  
15 in the San Juan Mountains, Colorado, 2011-2016: Compositional variability bearing on  
16 snow-melt effects, *Journal of Geophysical Research: Atmospheres*, n/a,  
17 e2019JD032210, 10.1029/2019JD032210, 2020.

18 Ricchiazzi, P., Yang, S. R., Gautier, C., and Sowle, D.: SBDART: A research and  
19 teaching software tool for plane-parallel radiative transfer in the Earth's atmosphere,  
20 *Bulletin of the American Meteorological Society*, 79, 2101-2114, 10.1175/1520-  
21 0477(1998)079<2101:Sarats>2.0.Co;2, 1998.

22 Shao, J. F., and Mao, J. D.: Dust Particle Size Distributions during Spring in Yinchuan,  
23 China, *Adv Meteorol*, 2016, 10.1155/2016/6940502, 2016.

24 Shao, Y. P., Wyrwoll, K. H., Chappell, A., Huang, J. P., Lin, Z. H., McTainsh, G. H.,  
25 Mikami, M., Tanaka, T. Y., Wang, X. L., and Yoon, S.: Dust cycle: An emerging core  
26 theme in Earth system science, *Aeolian Res*, 2, 181-204, 10.1016/j.aeolia.2011.02.001,  
27 2011.

28 Shi, T., Pu, W., Zhou, Y., Cui, J., Zhang, D., and Wang, X.: Albedo of Black Carbon-

1 Contaminated Snow Across Northwestern China and the Validation With Model  
2 Simulation, *Journal of Geophysical Research: Atmospheres*, 125, e2019JD032065,  
3 10.1029/2019JD032065, 2020.

4 Skiles, S. M., Flanner, M., Cook, J. M., Dumont, M., and Painter, T. H.: Radiative  
5 forcing by light-absorbing particles in snow, *Nat Clim Change*, 1, 10.1038/s41558-018-  
6 0296-5, 2018.

7 Spaulding, N. E., Meese, D. A., and Baker, I.: Advanced microstructural  
8 characterization of four East Antarctic firn/ice cores, *J Glaciol*, 57, 796-810,  
9 10.3189/002214311798043807, 2011.

10 Stamnes, K., Tsay, S. C., Wiscombe, W., and Jayaweera, K.: Numerically Stable  
11 Algorithm for Discrete-Ordinate-Method Radiative-Transfer in Multiple-Scattering  
12 and Emitting Layered Media, *Appl Optics*, 27, 2502-2509, 10.1364/Ao.27.002502,  
13 1988.

14 Usha, K. H., Nair, V. S., and Babu, S. S.: Modeling of aerosol induced snow albedo  
15 feedbacks over the Himalayas and its implications on regional climate, *Climate*  
16 *Dynamics*, 10.1007/s00382-020-05222-5, 2020.

17 Velesco, N., Kaiser, T., and Schweiger, G.: Computation of the internal field of a large  
18 spherical particle by use of the geometrical-optics approximation, *Appl Optics*, 36,  
19 8724-8728, 10.1364/AO.36.008724, 1997.

20 Wagner, R., Ajtai, T., Kandler, K., Lieke, K., Linke, C., Müller, T., Schnaiter, M., and  
21 Vragel, M.: Complex refractive indices of Saharan dust samples at visible and near UV  
22 wavelengths: a laboratory study, *Atmos. Chem. Phys.*, 12, 2491-2512, 10.5194/acp-12-  
23 2491-2012, 2012.

24 Wang, X., Doherty, S. J., and Huang, J.: Black carbon and other light-absorbing  
25 impurities in snow across Northern China, *Journal of Geophysical Research:*  
26 *Atmospheres*, 118, 1471-1492, 10.1029/2012jd018291, 2013.

27 Wang, X., Pu, W., Ren, Y., Zhang, X., Zhang, X., Shi, J., Jin, H., Dai, M., and Chen, Q.:  
28 Observations and model simulations of snow albedo reduction in seasonal snow due to

1 insoluble light-absorbing particles during 2014 Chinese survey, *Atmos Chem Phys*, 17,  
2 2279-2296, 10.5194/acp-17-2279-2017, 2017.

3 Warren, S. G., and Wiscombe, W. J.: A Model for the Spectral Albedo of Snow .2. Snow  
4 Containing Atmospheric Aerosols, *J Atmos Sci*, 37, 2734-2745, 10.1175/1520-  
5 0469(1980)037<2734:Amftsa>2.0.Co;2, 1980.

6 Warren, S. G.: Impurities in Snow - Effects on Albedo and Snowmelt Review, *Ann  
7 Glaciol*, 5, 177-179, 10.3189/1984AoG5-1-177-179, 1984.

8 Warren, S. G., Brandt, R. E., and Grenfell, T. C.: Visible and near-ultraviolet absorption  
9 spectrum of ice from transmission of solar radiation into snow, *Appl Optics*, 45, 5320-  
10 5334, 10.1364/Ao.45.005320, 2006.

11 Warren, S. G., and Brandt, R. E.: Optical constants of ice from the ultraviolet to the  
12 microwave: A revised compilation, *J Geophys Res-Atmos*, 113,  
13 10.1029/2007JD009744, 2008.

14 Warren, S. G.: Optical properties of ice and snow, *Philos T R Soc A*, 377,  
15 10.1098/rsta.2018.0161, 2019.

16 Xie, X. N., Liu, X. D., Che, H. Z., Xie, X. X., Li, X. Z., Shi, Z. G., Wang, H. L., Zhao,  
17 T. L., and Liu, Y. G.: Radiative feedbacks of dust in snow over eastern Asia in CAM4-  
18 BAM, *Atmos Chem Phys*, 18, 12683-12698, 10.5194/acp-18-12683-2018, 2018.

19 Yao, T. D., Masson-Delmotte, V., Gao, J., Yu, W. S., Yang, X. X., Risi, C., Sturm, C.,  
20 Werner, M., Zhao, H. B., He, Y., Ren, W., Tian, L. D., Shi, C. M., and Hou, S. G.: A  
21 review of climatic controls on  $\delta^{18}\text{O}$  in precipitation over the Tibetan Plateau:  
22 Observations and simulations, *Reviews of Geophysics*, 51, 10.1002/rog.20023, 2013.

23 Yasunari, T. J., Koster, R. D., Lau, K. M., Aoki, T., Sud, Y. C., Yamazaki, T., Motoyoshi,  
24 H., and Kodama, Y.: Influence of dust and black carbon on the snow albedo in the  
25 NASA Goddard Earth Observing System version 5 land surface model, *J Geophys Res-  
26 Atmos*, 117, 10.1029/2012jd018691, 2012.

27 Yasunari, T. J., Koster, R. D., Lau, W. K. M., and Kim, K. M.: Impact of snow darkening  
28 via dust, black carbon, and organic carbon on boreal spring climate in the Earth system,



1 J Geophys Res-Atmos, 120, 5485-5503, 10.1002/2014jd022977, 2015.

2 Zege, E. P., Ivanov, A. P., and Katsev, I. L.: Image transfer through a scattering medium.  
3 Berlin, Springer-Verlag, 1991.

4 Zender, C. S., Bian, H. S., and Newman, D.: Mineral Dust Entrainment and Deposition  
5 (DEAD) model: Description and 1990s dust climatology, J Geophys Res-Atmos, 108,  
6 10.1029/2002JD002775, 2003.

7 Zhang, D., Iwasaka, Y., Shi, G., Zang, J., Matsuki, A., and Trochkin, D.: Mixture state  
8 and size of Asian dust particles collected at southwestern Japan in spring 2000, Journal  
9 of Geophysical Research: Atmospheres, 108, 10.1029/2003JD003869, 2003.

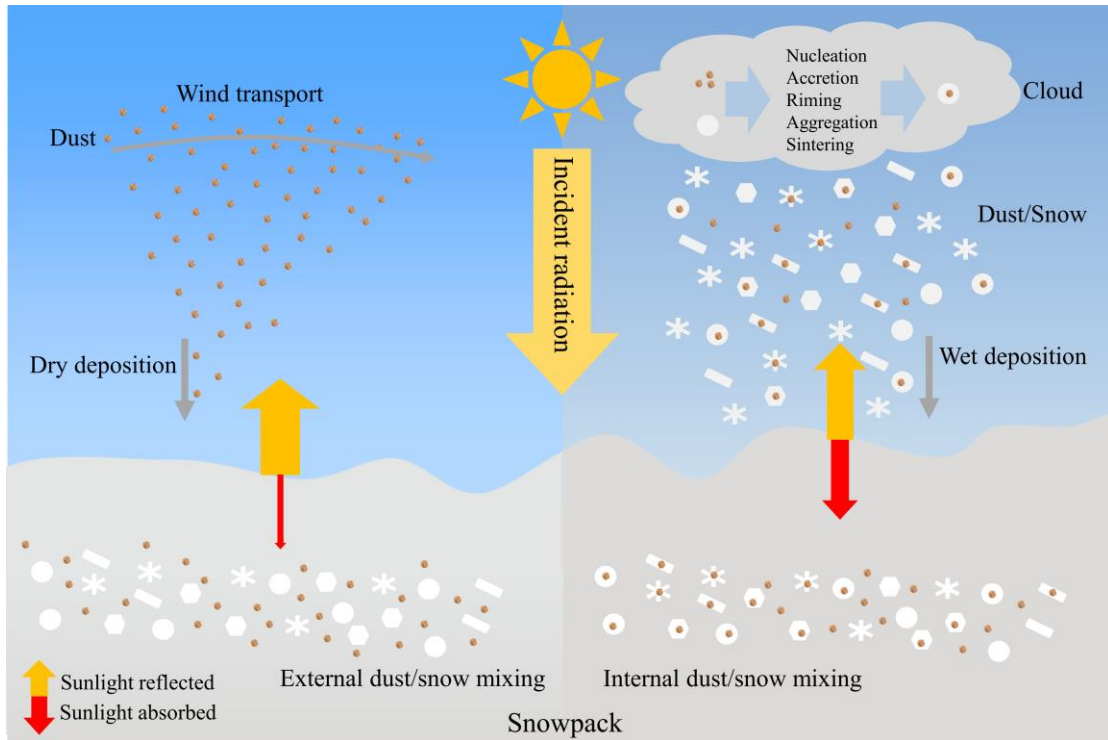
10 Zhang, Y. L., Kang, S. C., Cong, Z. Y., Schmale, J., Sprenger, M., Li, C. L., Yang, W.,  
11 Gao, T. G., Sillanpaa, M., Li, X. F., Liu, Y. J., Chen, P. F., and Zhang, X. L.: Light-  
12 absorbing impurities enhance glacier albedo reduction in the southeastern Tibetan  
13 plateau, J Geophys Res-Atmos, 122, 6915-6933, 10.1002/2016jd026397, 2017.

14 Zhang, Y. L., Kang, S. C., Sprenger, M., Cong, Z. Y., Gao, T. G., Li, C. L., Tao, S., Li,  
15 X. F., Zhong, X. Y., Xu, M., Meng, W. J., Neupane, B., Qin, X., and Sillanpaa, M.:  
16 Black carbon and mineral dust in snow cover on the Tibetan Plateau, Cryosphere, 12,  
17 413-431, 10.5194/tc-12-413-2018, 2018.

18 Zhao, C., Hu, Z., Qian, Y., Leung, L. R., Huang, J., Huang, M., Jin, J., Flanner, M. G.,  
19 Zhang, R., Wang, H., Yan, H., Lu, Z., and Streets, D. G.: Simulating black carbon and  
20 dust and their radiative forcing in seasonal snow: a case study over North China with  
21 field campaign measurements, Atmos Chem Phys, 14, 11475-11491, 10.5194/acp-14-  
22 11475-2014, 2014.

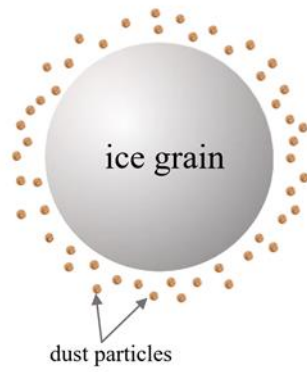
23 Zhou, X. B., Li, S. S., and Stamnes, K.: Effects of vertical inhomogeneity on snow  
24 spectral albedo and its implication for optical remote sensing of snow, J Geophys Res-  
25 Atmos, 108, 10.1029/2003JD003859, 2003.

26

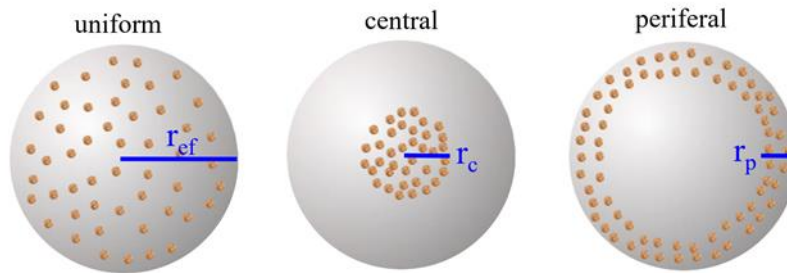


1  
 2 **Figure 1.** Schematic of dust mixing with snow grains internally. Dust tends to mix  
 3 externally with snow grains through dry deposition and/or below cloud scavenging,  
 4 while dust–snow internal mixtures can be produced by nucleation, accretion, riming,  
 5 aggregation, and sintering during aerosol–cloud–precipitation processes known as wet  
 6 deposition. Arrows represent how the absorption (red) and reflection (yellow) of  
 7 incoming sunlight changes with dust–snow mixing state.  
 8

External dust/ice mixing (EDM)

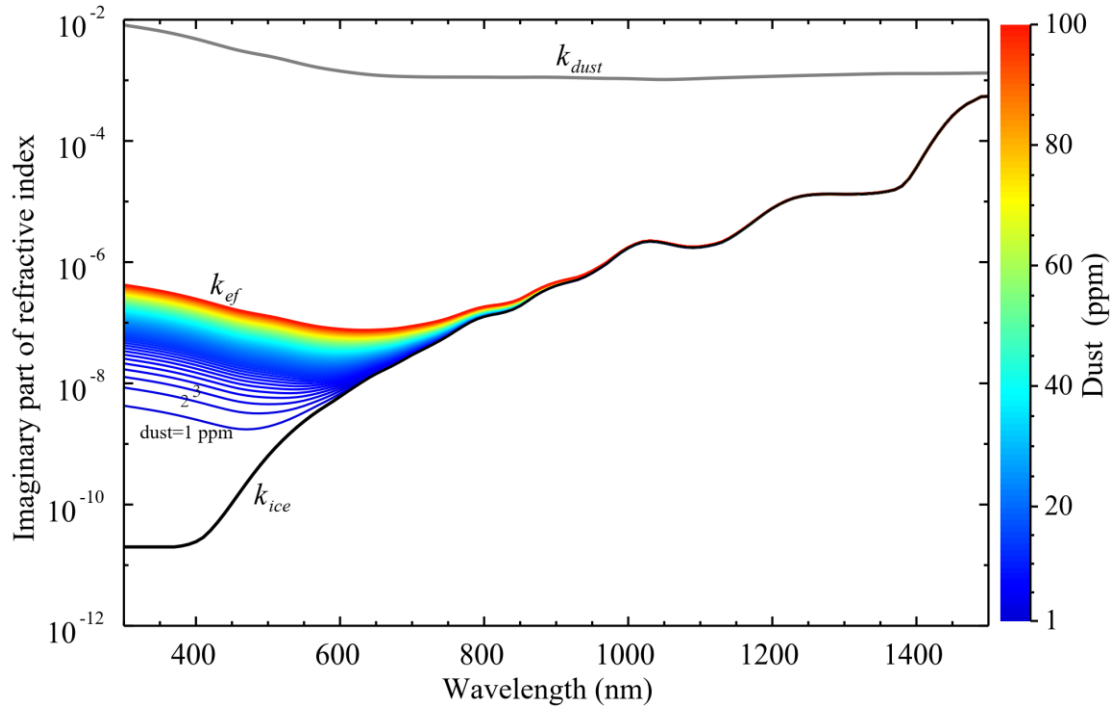


Internal dust/ice mixing (IDM)



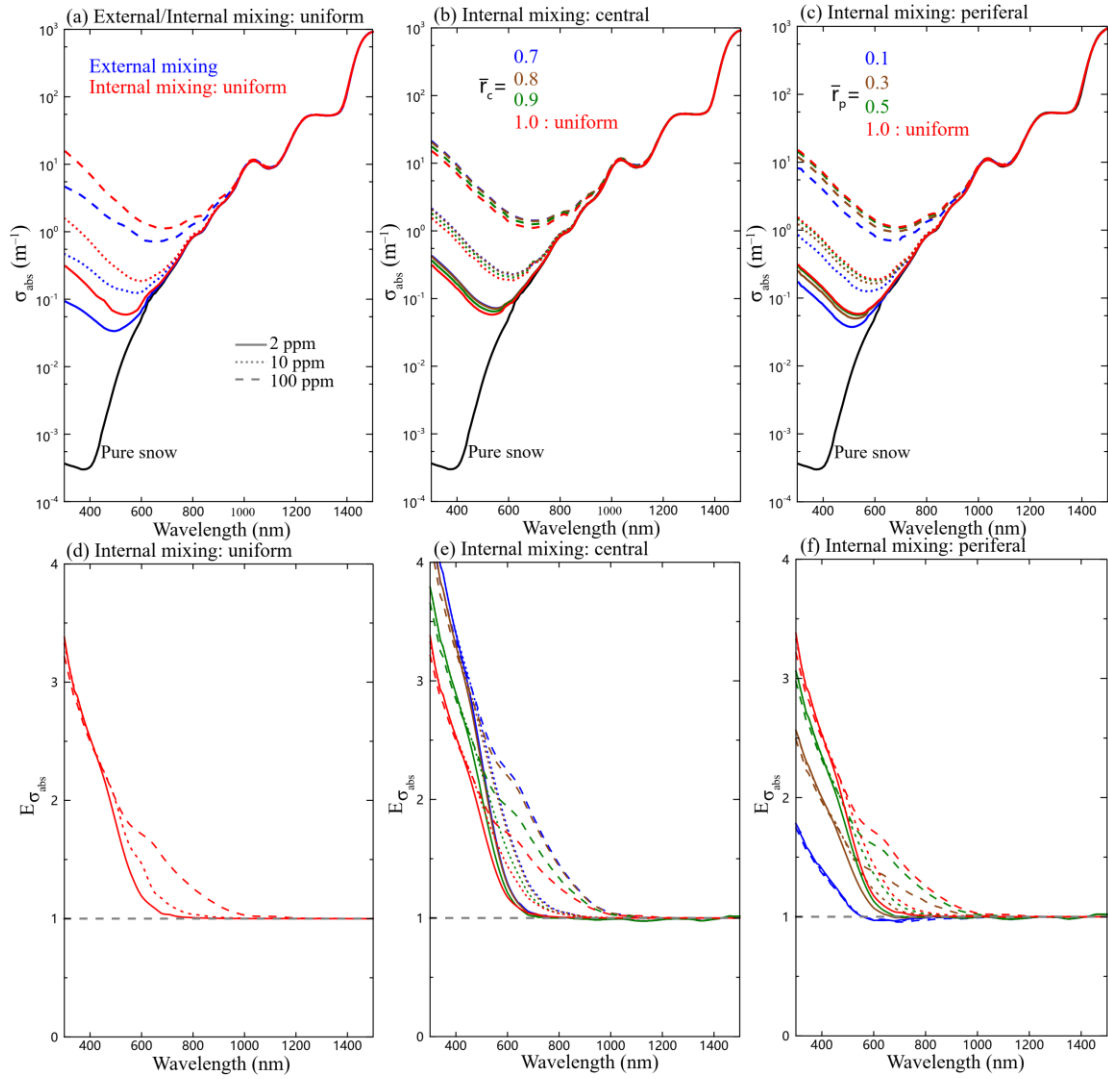
1  
2  
3  
4

**Figure 2.** Schematic depicting various mixing scenarios of snow grains and dust particles.

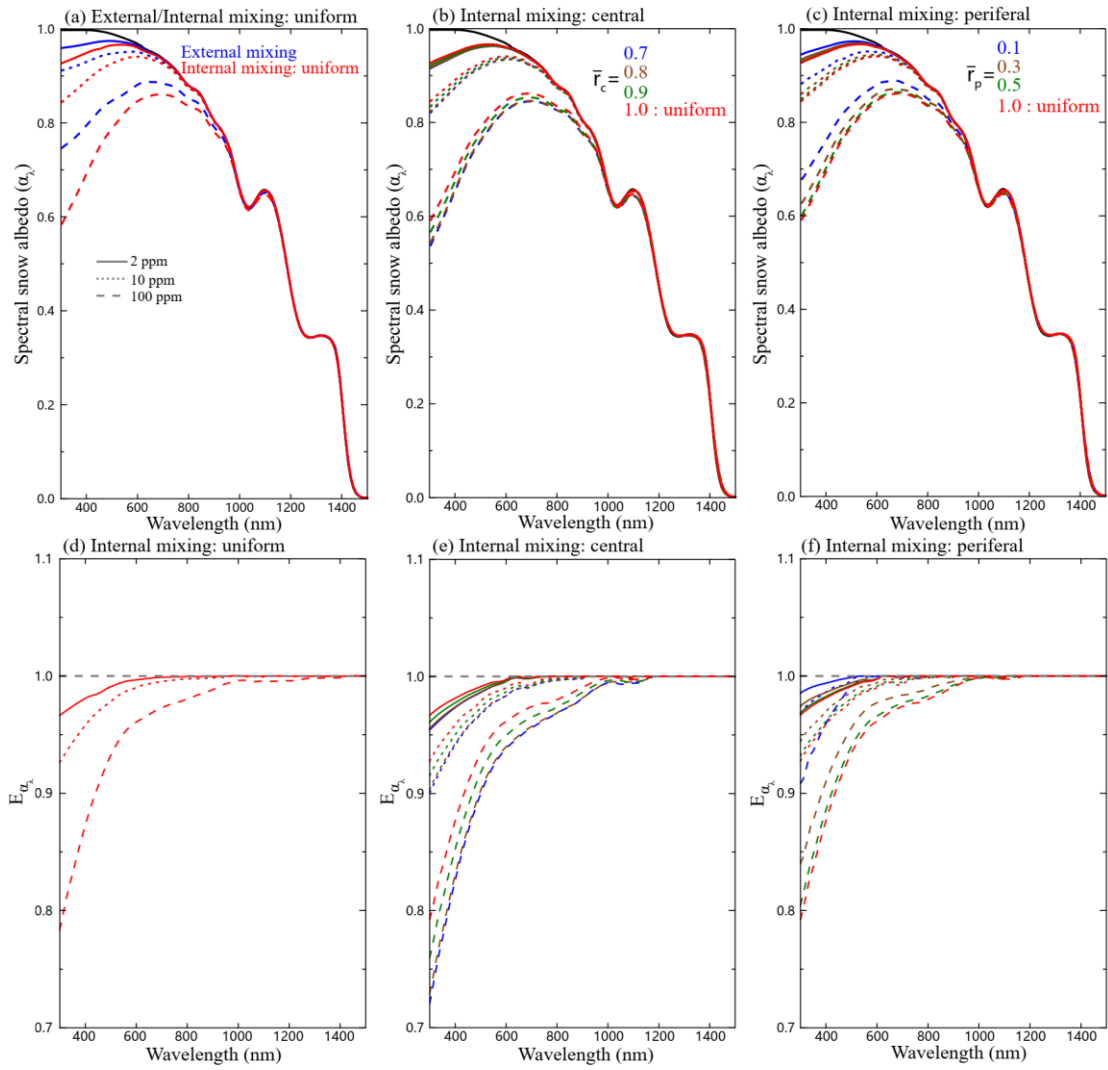


1  
2  
3  
4  
5  
6

**Figure 3.** Imaginary part of the spectral complex refractive indices of ice ( $k_{ice}$ ) and dust ( $k_{dust}$ ) (Warren and Brandt, 2008; Dang et al., 2015), with the imaginary part of the effective complex refractive indices ( $k_{ef}$ ) as a function of wavelength, at dust mass concentrations ( $C_{dust}^*$ ) of 1–100 ppm (or  $\mu\text{g g}^{-1}$ ) in snow.

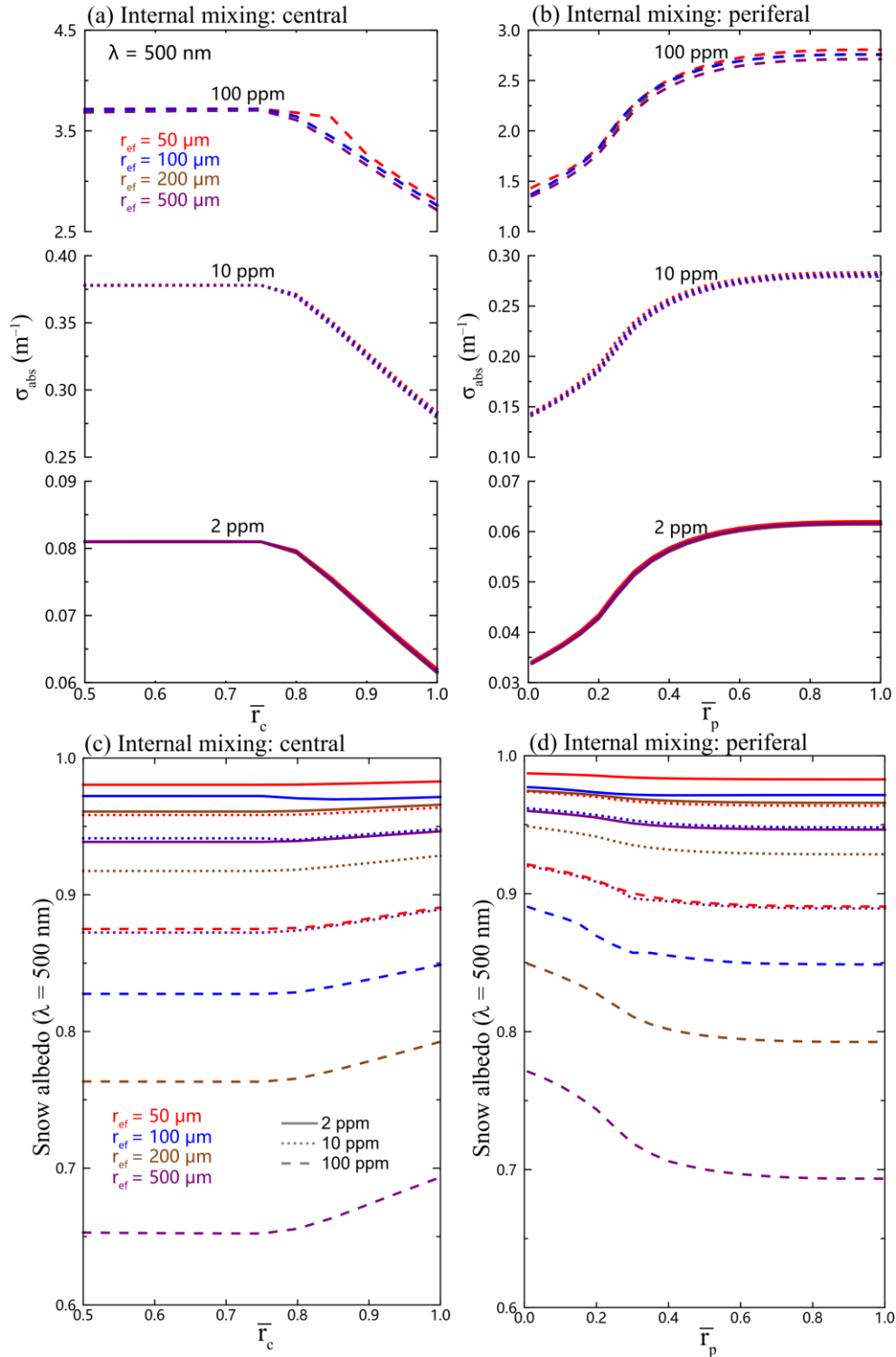


1  
2 **Figure 4.** Snow absorption coefficients ( $\sigma_{\text{abs}}$ ) for dust–snow (a) external and internal  
3 mixing (uniform), (b) internal mixing (central), and (c) internal mixing (peripheral), as  
4 a function of wavelength with different dust concentrations and  $\bar{r}_c$  and  $\bar{r}_p$ . The  
5 corresponding enhancement ( $E\sigma_{\text{abs}}$ ) caused by (d) internal mixing (uniform), (e) internal  
6 mixing (central), and (f) internal mixing (peripheral) relative to external mixing, is  
7 shown as a function of wavelength. The snow grain radius was assumed to be 200  $\mu\text{m}$ .  
8



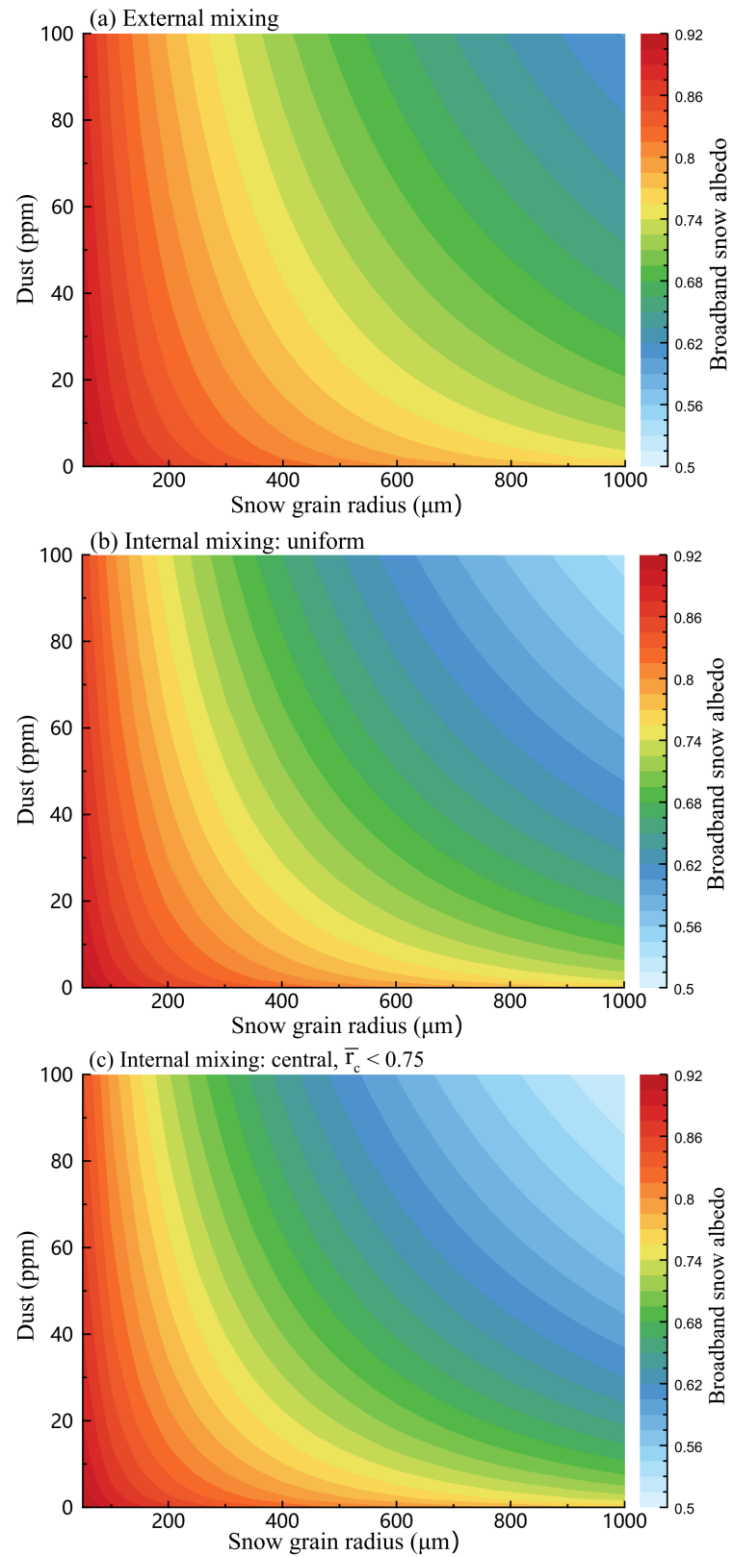
1  
2  
3

**Figure 5.** Same as Figure 4, but for spectral snow albedo ( $\alpha_\lambda$ ).



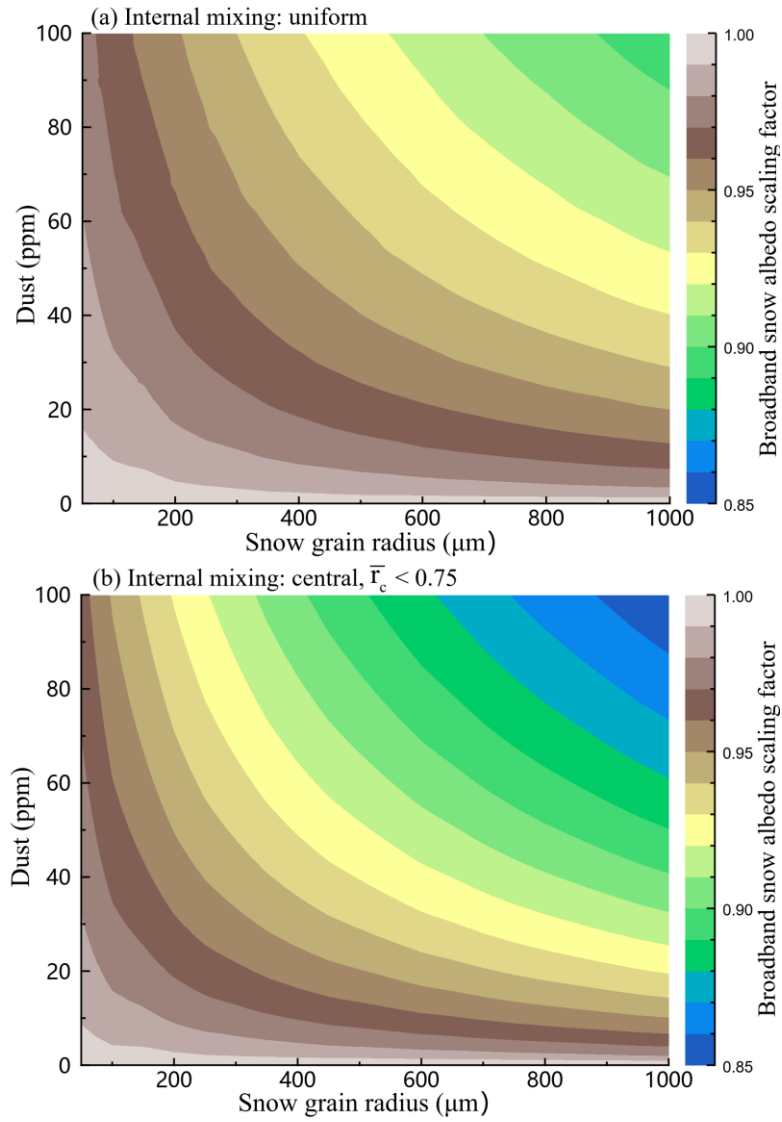
1  
2  
3  
4  
5  
6

**Figure 6.** The snow absorption coefficient ( $\sigma_{\text{abs}}$ ) at 500 nm wavelength as a function of  $\bar{r}_c$  and  $\bar{r}_p$  for (a) internal mixing (central) and (b) internal mixing (peripheral) with different snow grain radii and dust mass concentrations. (d) and (e) are the same as (a) and (b), but for snow albedo at 500 nm wavelength.

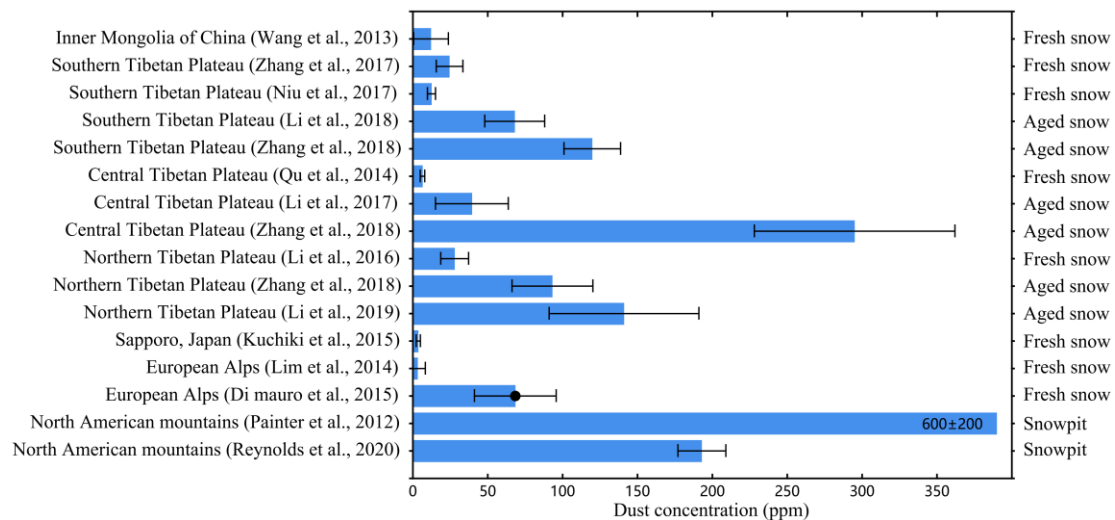


1  
2 **Figure 7.** Broadband snow albedo ( $\alpha_{\text{integrated}}$ ) variations affected by different dust  
3 mass concentrations and snow grain radii for (a) external mixing, (b) internal mixing  
4 (uniform), and (c) internal mixing (central,  $\bar{r}_c < 0.75$ ).  
5

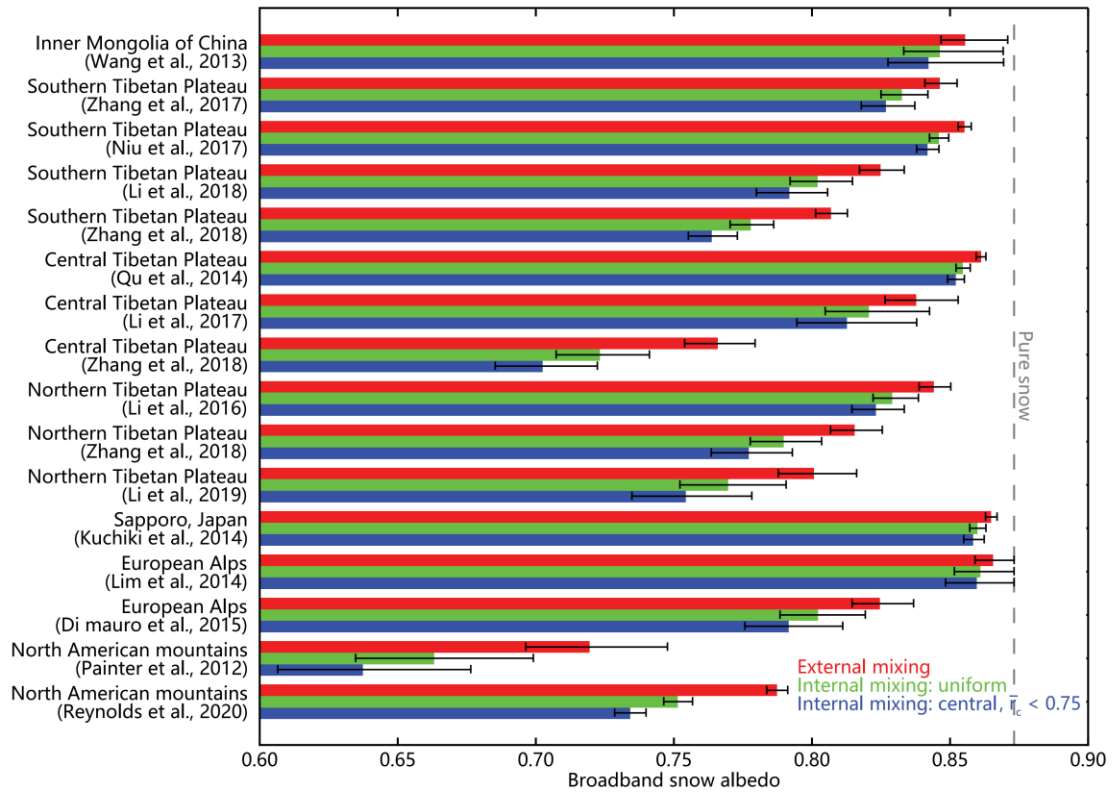




1  
 2 **Figure 8.** Variations in the broadband snow albedo scaling factor ( $E_{\alpha, \text{integrated}}$ , ratio of  
 3  $\alpha_{\text{integrated}}$  for IDM to EDM) due to different dust mass concentrations and snow grain  
 4 radii for (a) internal mixing (uniform) and (b) internal mixing (central,  $\bar{r}_c < 0.75$ ).  
 5

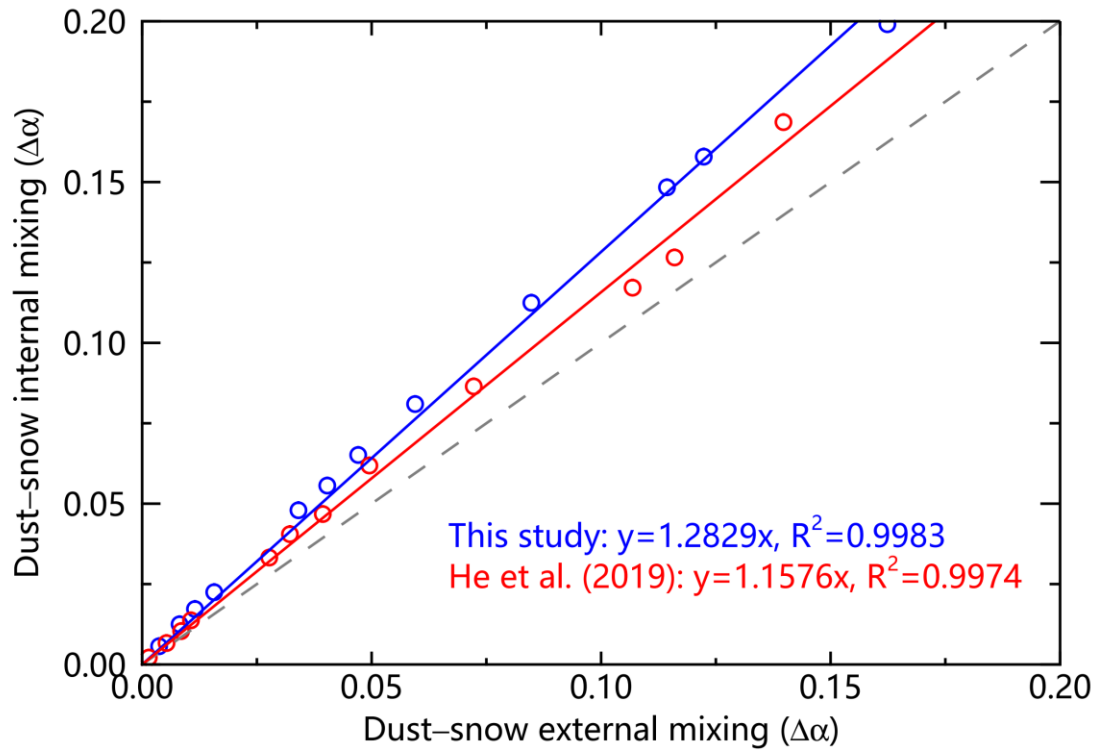


1  
2 **Figure 9.** In situ measurements of dust concentrations in snow (fresh snow, aged snow,  
3 and snowpit from field sampling in different regions of the Northern Hemisphere. The  
4 solid black circle represents snow samples that were collected days after a significant  
5 dust transport event.  
6



1

2 **Figure 10.** Calculated broadband snow albedo based on dust concentration  
 3 measurements in different areas for dust–snow external mixing, internal mixing  
 4 (uniform), and internal mixing (central,  $\bar{r}_c < 0.75$ ). The dashed line represents  
 5 broadband albedo of pure snow, and the snow grain radius was assumed to be 200  $\mu\text{m}$ .



1

2 **Figure 11.** Comparisons of snow albedo reduction ( $\Delta\alpha$ ) under the cloudy sky caused  
 3 by dust-snow uniform internal mixing (y-axis) and external mixing (x-axis) for this  
 4 study (blue) and He et al. (2019) (red).

5